DYNAMIC RESPONSE OF SIMPLY SUPPORTED BEAMS EXCITED BY PIEZOELECTRIC ACTUATORS

Jerome F. Rivory

Thesis submitted for the partial fulfilment of the degree of

Master of Engineering Science

in

The University of Adelaide

(Department of Mechanical Engineering)

TABLE OF CONTENTS

Abstract . . . . . (i)

Statement of originality . . . . . (ii)

Acknowledgments . . . . . (iii)

1.0 Introduction 1

2.0 Literature review 3

2.1 Models of structures excited by piezoelectric actuators 3

2.2 Power flow measurements in beams 5

3.0 Response of beams excited by piezoelectric actuators 9

3.1 Review of existing models 9

3.2 Corrected dynamic system model 20

3.3 Comparison of experimental and analytical results for a thin beam 28

3.3.1 Experimental set-up and computation of data 28

3.3.2 Results and discussion 36

3.4 Comparison of experimental and analytical results for a thick beam 47

3.4.1 Experimental set-up and computation of data 47

3.4.2 Results and discussion 52

4.0 Power flow and coupling efficiency for a thin beam 59

4.1 Theory of power flow measurements in beams 59

4.1.1 Flexural wave power flow measurements 59

4.1.2 Power flow in electrical devices 62

4.1.3 Mechanical power flow using a force transducer and an accelerometer 63

4.1.4 Coupling efficiency 63

4.2 Power flow measurements in a thin beam excited by piezoelectric actuators 64

4.2.1 Experimental set-up 64

4.2.2 Results and discussion 66

4.3 Power flow measurements in a thin beam excited by an electromechanical shaker 70

4.3.1 Experimental set-up 70

4.3.2 Results and discussion 70

5.0 Other considerations 76

5.1 Piezoelectric actuator failures 76

5.2 Actuator voltage linearity 79

5.3 Actuator leakage 81

5.4 Actuator non-linearities 81

5.5 Shear lag - strain singularity 83

6.0 Conclusions and recommendations 85

References 88

List of symbols 93

ABSTRACT

The use of piezoelectric devices for the purposes of active noise or vibration control has become attractive in recent times. These small, power to weight efficient devices have had some success in active vibration control; however, the force transfer mechanism by which they interact with the structure to which they are attached needs to be understood to optimise the efficiency of their use.

Various modelling approaches have been used over the past six (6) years to try and understand the force transfer mechanism in beams and plates, and in this work an adaptation of a published model is presented, and compared with experimental data and other published models.

The force transfer mechanism between the piezoelectric actuator and the beam is found to be dependent upon the impedance of the beam. At resonance, the free edge condition of the piezoelectric actuator does not affect the strain field close to the free edge. Away from resonances, the force transfer mechanism is different and less efficient, and the free edge condition of the piezoelectric actuator does affect the strain field close to the free edge of the actuator.

Further experimental work, investigating the power flow from the piezoelectric actuators to the beam, emphasises some of the differences found between the theory and experiments, and between the performance of piezoelectric actuators and electrodynamic actuators.

STATEMENT OF ORIGINALITY

This work contains no material which has been accepted for the award of any other degree or diploma in any university or other tertiary institution and, to the best of my knowledge and belief, contains no material previously published or written by another person, except where due reference has been made in the text.

I give consent to this copy of my thesis, when deposited in the University Library, being available for loan and photocopying.

SIGNED: ... . DATE: ...12-8-92.....

ACKNOWLEDGMENTS

It is with sincere gratitude that I would like to thank all who helped and encouraged me throughout the time it took to undertake this thesis. In particular, I would like to thank my supervisor, Dr. Colin Hansen, without whom this project would not have taken place, both for his support in technical matters and his help is securing financial support.

I thank the University of Adelaide, whose non-smoking policy and its largely non-smoking population for giving me the chance to quit, and remain a non-smoker.

I thank the Sir Ross and Sir Keith Smith Fund for providing the scholarship which made this work possible.

A number of people assisted me in various ways, and I would like to thank Dr. Yitshak Ram for some invaluable help with differential equations, George Osborne for his patience when replacing blown piezoelectric crystals, all the other post-graduate students and staff in the Department of Mechanical Engineering, who made it a pleasure to turn up for work.

Lastly, but not least, my heart-felt thanks go to my wife Robyn and my daughter Hannah for their support and patience.

1.0 INTRODUCTION

In recent times there has been a substantial amount of interest generated in the use of piezoelectric actuators for structural and acoustic control. (Bailey and Hubbard Jr., 1985; Crawley and de Luis, 1987; Burke and Hubbard Jr, 1988; Baz and Poh, 1988; Fuller *et al.*, 1989; Liang and Rogers, 1989; Pan and Hansen, 1989 and 1990; Hansen and Pan, 1990; Wang *et al.*, 1990; Liao and Sung, 1991; Rogers *et al.*, 1991). For the purposes of active vibration and noise control, piezoelectric devices have shown great potential as actuators or sensors, because they are inexpensive, small and lightweight, and can be easily bonded to or into any structure. They are spatially distributed and thus cannot be modelled as point force excitations. This latter characteristic demands that new and special modelling techniques be used to estimate the response of structures driven by them.

The remainder of this thesis begins with a review of previously published work on the use of piezoelectric crystals as actuators on beams and plates. In particular, work done by Pan and others at the University of Adelaide which involves an attempt to obtain a valid, exact, classical model for the response of a beam excited in pure bending by a pair of out of phase piezoelectric actuators is discussed in detail.

The review of previous work is followed by the presentation of a corrected model which is compared to experimental data and to other published theoretical models.Differences between the experimental data and the theoretical models are discussed and explanations are given for some of these differences.

Finally, the coupling efficiency, defined as the electrical input over the mechanical power output of piezoelectric actuators is compared experimentally to that of an electrodynamic shaker on a thin beam. The results of these tests are discussed and some of the measurement difficulties are highlighted.

2.0 LITERATURE REVIEW

2.1 Models of structures excited by piezoelectric actuators

A good review of past work on the usage of piezoelectric actuators has been written by Smits *et al.* and the constitutive piezoelectric equations which describe the three dimensional strain and electrical field within piezoelectric materials, can be found in texts such as Kino (1987). In the published models reviewed here, and in the model presented here, the simplified one dimensional version of these constitutive equations is used, and these will be discussed in Section 3.0.

The first important study concerned with modelling the performance of piezoelectric actuators bonded to a beam was a static analysis (Crawley and de Luis, 1987) in which four assumed piezoelectric-substructure strain distributions, were used. Two of these distributions were static elastic models describing beam extension using embedded and surface mounted piezoelectric actuators. The other two distributions described beam bending using embedded and surface mounted piezoelectric actuators. The model, describing beam bending using surface mounted piezoelectric actuators, assumed a uniform strain distribution across the actuator thickness, and thus did not account for actuator bending. The loading mechanism was found to be a linear function of the actuator stress-free strain. A shear lag mechanism was identified as being responsible for force transfer between the piezoelectric actuator and the beam. The static analysis was then further extended to dynamic analysis using the Rayleigh-Ritz approach.

Crawley and Anderson, 1990, rectified the problems with the assumed uniform strain model by presenting a Bernoulli-Euler static model (which neglects the effects of transverse shear and rotary inertia) of the beam/actuator system which did take the actuator bending into account, and hence had a strain distribution across the actuator thickness which varied linearly with distance from the central axis of the beam. A finite element static model showed that the new assumption was correct. Further, this FE model showed the extensional strain distributions on the top of the actuator, on the top of the beam, and at the centre of the beam. Unfortunately, the experimental results presented failed to confirm the predicted distributions. The authors also discussed some non-linear characteristics of piezoelectric crystal actuators, such as the lack of linearity between the developed strain and the input field voltage, and hysteretic losses during loading and unloading of the piezoelectric actuators.

Another important model (Burke and Hubbard, 1987) examined the dynamic behaviour of a beam by applying a spatially distributed constant strain, using step functions, onto a modal expansion of the beam response. Later they extended their theoretical work, using spatially-varying discontinuity functions, to include spatially-varying actuator distributions on beams to achieve modal vibration control (Burke and Hubbard, 1988). However, this work did not consider the actual force transfer mechanism between actuator and beam.

Clark *et al.*, 1991, also considered the use of step moment excitation and a modal representation of the beam response to achieve a dynamic prediction of the beam response. Their model used a similar approach to Crawley and Anderson, 1990, to define the extensional strain distribution at the crystal/beam interface, but the incorrect assumption

that the linear variation of stress across the beam thickness has the same slope as the variation across the actuator thickness limited the usefulness of the model.

A similar modelling approach, with the same incorrect assumption, has also been used by Dimitriadis *et al.* (1991) to predict the dynamic response of a two dimensional thin plate excited by a pair of piezoelectric actuators.

Kim and Jones, 1991, extended the work of Dimitriadis *et al.* by correcting the assumption of identical stress slopes across the beam and actuator thicknesses, and allowing for the effect of a glue layer between the plate and the actuators.

Pan *et al.* (1992) attempted to obtain a valid, exact, classical model for the response of a beam excited in pure bending by a pair of piezoelectric actuators. In this paper, this work is corrected and extended to obtain a theoretical solution to this problem, and experimental data to support and extend this work are also presented.

2.2 Power flow measurements in beams

The idea of measuring the vibrational intensity (power flow per unit width) in plates and beams was first presented by Noiseux, 1970, who introduced the idea that there exists a far and near-field of intensity. The near-field intensity is in the region of the actuator, and contains a reactive and active component. A purely reactive intensity component is a component where the particle force and velocity are out of phase, and a purely active intensity component is where the force and velocity are in phase, and thus is a real

quantity. The reactive intensity component decays rapidly away from the region of force input, although in reverberant fields, ie. in the presence of standing waves, there will be a large component of reactive intensity. The active intensity has two components, a force component which is due to shear waves and a moment component which is due to flexural waves. Noiseux, 1970, showed that in the far-field the intensity contributions from the force component and the moment component are equal and are each exactly half of the total intensity.

Techniques for the measurement of surface intensity, using accelerometers, were presented by Pavic (1976) who showed, using finite difference approximations, that all quantities relating to intensity flows in both one and two-dimensional flexural wave models can be calculated. The finite difference scheme developed by Pavic enabled an estimation to be made of the third order spatial derivative, necessary for near field measurement of active intensity, using four measurement points. Thus four accelerometers were required for near-field power estimation. In the far-field it was shown that, since the force and moment components are equal, and the moment component is only a second order spatial derivative, power estimation only requires two accelerometers. Time integrals and multiplication of signals were achieved using analog equipment.

As the signal processing capabilities of spectrum analysers improved, the time integration and multiplication of signals could be carried out in the frequency domain (Verheij, 1980). As shown by Verheij, all Pavic's power relationships have frequency domain equivalents which can be evaluated using the cross-spectrum capability of a two channel spectrum analyser.

Carles *et al.* showed that accelerometers and strain gauges could be used to estimate near-field power flow in beams (Carles *et al.*, 1983). This was achieved using a finite difference scheme based on two measurement points. Their far-field scheme was the same as that of Pavic (1976).

Further finite difference schemes were highlighted by Hayek *et al.*, 1990. To try to isolate the mass loading effects of accelerometers, this group used a scanning laser to measure the required quantities. It was also shown that if a measurement point separation of a twentieth of a wavelength was used, then less than a 0.3 dB error in the near-field and 0.1 dB error in the far-field existed between the results of Pavic's scheme and the results of all their other more sophisticated schemes (some of which were 7 point schemes). Importantly, errors due to both random phase and amplitude shifts were presented, and shown to be significant.

Practical limitations of the four measurement point finite difference scheme were investigated by Taylor, 1990. In this paper, the one dimensional beam equation was solved and from this solution the exact power flow in the beam could be calculated and compared to simulated results using the four point scheme. Four parameters were found to have significant effects on the results obtained using the finite difference scheme. These were the finite difference approximation itself, the relative phase accuracy between transducers, the achievable accuracy in transducer spacing, and the reverberation level of the structure. Taylor showed that the finite difference approximation error was minimised for small transducer separations (approximately a twentieth of a wavelength), but that the errors due

to the other parameters were in fact maximised for small transducer separations (Taylor, 1990). Another important finding was that for structures with high reverberation and/or high measurement phase errors, the error in the power flow measured by the four point scheme may in fact be so large as to be opposite in sign to the true power flow (Taylor, 1990).

3.0 RESPONSE OF BEAMS EXCITED BY PIEZOELECTRIC ACTUATORS

3.1 Review of existing models

Any voltage applied to piezoelectric actuators bonded to the upper and lower surfaces of a beam will generate surface extensions, the direction of which will be determined by the poling direction of the piezoelectric actuators and the polarity of the applied voltage. Should both the lower and upper actuators undergo positive or negative extensions then the beam will undergo, respectively, positive or negative longitudinal extensions. Should the upper actuator undergo a positive extension while the lower actuator undergoes a negative extension or vice versa, the beam will bend (Figure 1).

An equivalent system can be obtained if the actuators are replaced by a pair of counteracting line moments as shown in Figure 2.

Constitutive equations describe piezoelectric materials using five independent elastic constants, and three piezoelectric constants. Three dimensional constitutive equations can be reduced to the following one dimensional form, which for an actuator polarised across its thickness t_c can be written as:

$$\varepsilon_c = d \frac{V}{t_c} + \frac{\sigma_c}{E_c} \tag{1}$$

$$D = \varepsilon_c^T \frac{V}{t_c} + d\, \sigma_c \tag{2}$$

where:

ε_c = actuator strain, d = piezoelectric stress constant, E_c = Young's modulus, V = voltage across actuator, σ_c = actuator stress, D = electric displacement, $\varepsilon^T{}_c$ = stress free permittivity.

In low frequency (typically below a few kilohertz) usage, a voltage applied in the z direction of a three dimensional crystal (Figure 3) induces three normal strains (in terms of d_{33} and d_{31}), as follows:

$$\text{Direct strain} \quad \frac{\Delta t_c}{t_c} = \frac{V}{t_c} d_{33} \tag{3}$$

$$\text{Transverse strain} \quad \frac{\Delta L_c}{L_c} = \frac{\Delta b_c}{b_c} = \frac{V}{t_c} d_{31} \tag{4}$$

In considering the dynamic response of a beam to which piezoelectric actuators have been bonded, the constitutive equations can be further simplified, by only considering the strain equation, equation (1), and rewriting it in terms of stress:

$$\sigma_c = E_c(\varepsilon_c - \Lambda) \tag{5}$$

where:

$$\Lambda = \frac{V}{t_c} d_{31} \tag{6}$$

Considering pure bending deformation in the region of the actuators, the strain and stress distributions are linear as shown in Figure 4. Thus, the actuator/beam force transfer mechanism could be thought of as an applied strain distribution to each of the beam surfaces with the distribution on one surface 180^o out of phase to that on the other surface.

It is apparent that there are two possible equivalent force transfer mechanisms:

- Uniform out of phase surface strain distribution (ε^s_a) applied over the top and bottom surfaces of the actuator field

- Two counteracting external line moments (M_z) at each end of the actuator

It can be argued that the postulated equivalent transfer mechanisms are one and the same

and ignoring near-field effects, they can be used to predict far-field dynamic strain distributions (Kim and Jones, 1991; Clark *et al.*, 1991; Dimitriadis *et al.*, 1991; and Pan *et al.*, 1992). The externally induced surface strain on the beam acts to rotate a plane perpendicular to the x-axis, generating in the beam an internal moment M_x, over the width of the actuator, given by:

$$M_x = b_b \int_{-\frac{t_b}{2}}^{\frac{t_b}{2}} \sigma_x z\, dz = \frac{2b_b}{3}\left(\frac{t_b}{2}\right)^2 (\sigma_b^s) = \frac{b_b}{6}\, t_b^2\, E_b\, \varepsilon_a^s \qquad (7)$$

This internal moment M_x can also be generated by an equivalent external line moment M_z acting at the edge of the actuator and controlled by a similar moment acting in the opposite direction at the other edge. And thus the postulated transfer mechanisms are seen to be equivalent.

The model presented in this thesis uses a uniform extensional strain distribution, ε^s_a, over the specific actuator area to calculate the beam response. Furthermore, the model presented in this thesis does not reconsider the modelling of the applied strain distribution; rather, the model uses the results obtained by Crawley and Anderson (1990), although results from this model are compared to results obtained from Clark *et al.* (1991). The value obtained for the uniform extensional strain distribution, ε^s_a, will vary from model to model, mainly due to the underlying assumptions.

The assumption made by Clark *et al.* that the stress slope through the beam is the same as

that through the crystal, results in this model slightly underestimating (in the worst case, by less than 4% for one of the cases presented here) the applied strain distribution, ε^{s}_{a}. This is corrected in other models (Crawley and Anderson, 1990, and Kim and Jones, 1991).

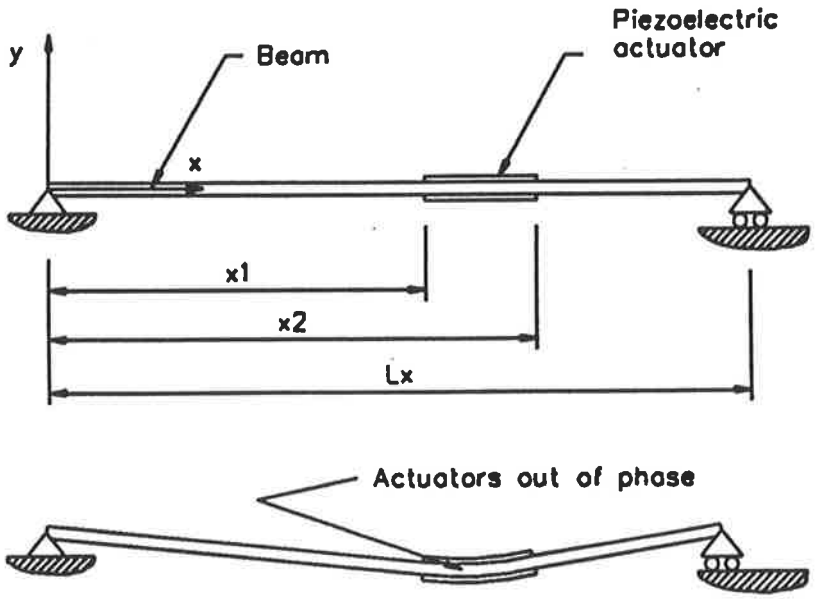

Figure 1. Simply supported beam with and without actuation

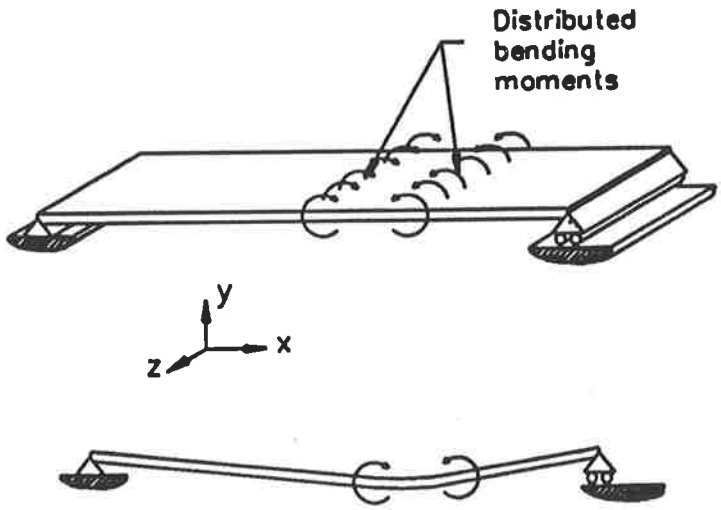

Figure 2. Equivalent system with distributed bending moments

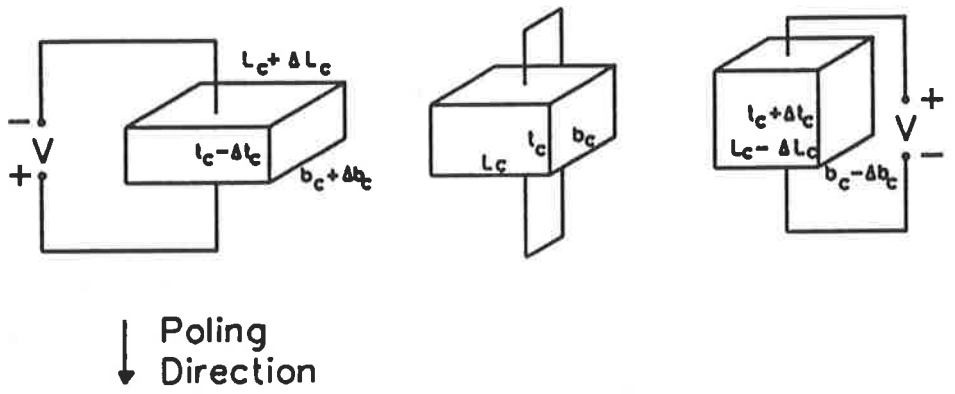

Figure 3. Extension of a piezoelectric crystal as a function of applied voltage

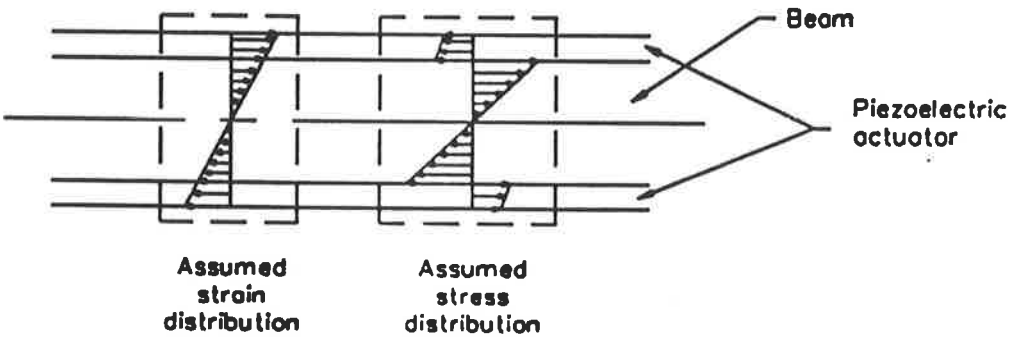

Figure 4. Strain and stress distributions across the beam and actuator system

The expressions for calculating the uniform strain ε^s_a applied to the beam using the various published models can be compared, by using the equivalence of the applied mechanisms defined by equation (7). In some cases, two dimensional plate models are reduced to one dimensional models to enable this comparison.

Crawley and de Luis (1987)

$$\varepsilon^s_a = \frac{6\Lambda}{6+\Psi_b} \tag{8}$$

where:

$$\Psi_b = \frac{E_b b_b t_b}{E_c b_c t_c} \tag{9}$$

Crawley and Anderson (1990)

$$\varepsilon^s_a = \frac{6(t_b+t_c)t_b\Lambda}{\left(\left(\frac{E_b t_b b_b}{E_c t_c b_c}\right)+6\right)t_b^2+12t_b t_c+8t_c^2} \tag{10}$$

Kim and Jones (1991)

For the special case, where the bonding layer is disregarded, where the two dimensional plate model is reduced to a one dimensional beam model, and where the beam width b_b and actuator width b_c are the same:

$$\varepsilon_a^s = \frac{\frac{3}{4}\frac{E_c}{E_b}\frac{1}{(1-\nu_c)}(t_b+t_c)t_b t_c \Lambda}{\left[\frac{t_b^3}{8}+\left(\frac{1-\nu_b}{1-\nu_c}\right)\frac{E_c t_c}{E_b}\left(\frac{3t_b^2}{4}+t_c^2+\frac{3t_b t_c}{2}\right)\right]} \tag{11}$$

Clark, Fuller and Wicks (1991)

$$\varepsilon_a^s = -\frac{P}{(1-P)}\Lambda \tag{12}$$

where:

$$P = -\frac{E_c}{E_b}K \tag{13}$$

$$K = \frac{3(t_b+t_c)t_b t_c}{4\left(\frac{t_b^3}{8}+t_c^3\right)+3t_b t_c^2} \tag{14}$$

Dimitriadis and Fuller (1991)

$$\varepsilon_a^s = \frac{-(1+\nu_c)P}{1+\nu_b-(1+\nu_c)P}\Lambda \tag{15}$$

where:

$$P = -\frac{E_c\,(1-\nu_b^2)}{E_b\,(1-\nu_c^2)}K \tag{16}$$

and

$$K = \frac{3t_c t_b(t_b+t_c)}{4\left(\frac{t_b^3}{8}+t_c^3\right)+3t_b t_c^2} \tag{17}$$

Pan, Hansen, and Snyder (1992)

$$\varepsilon_a^s = \Lambda \tag{18}$$

It should be noted that out of the above expressions, only equation (10) from Crawley and Anderson can be utilised when the beam and piezoelectric widths are not equal. The expressions derived by Clark, Fuller and Wicks (equations (12), (13), and (14)) can be extended to take the beam and actuator widths into account, as follows:

$$\varepsilon_a^s = -\frac{P}{(1-P)}\Lambda \tag{19}$$

where:

$$P = -\frac{E_c b_c}{E_b b_b}K \tag{20}$$

$$K = \frac{3(t_b+t_c)t_b t_c}{4\left(\frac{t_b^3}{8}+t_c^3\right)+3t_b t_c^2} \tag{21}$$

3.2 Corrected dynamic system model

Figure 5 shows a Bernoulli-Euler beam (for which the effects of transverse shear and rotary inertia are neglected) with an identical piezoelectric actuator mounted on opposite sides of the beam. In the model in Figure 5, the actuators are driven by a pair of electric fields with the same amplitude but of opposite phase. The actuators are perfectly bonded to the beam, and as discussed in the introduction, it is possible to replace their effect by a uniform strain distribution over their areas. The beam system can be analysed as three separate beams.

The Bernoulli-Euler beam equation is (Thompson, 1981):

$$E_b I_b \frac{\partial^4 y}{\partial^4 x} - m_b' \frac{\partial^2 y}{\partial^2 t} = 0 \qquad (22)$$

where:

$$m_b' = \rho_b b_b t_b \qquad (23)$$

The angular displacement θ of the cross section plane normal to the beam axis can be calculated by:

$$\theta = \frac{\partial y}{\partial x} = -\frac{2u_b^s}{t_b} \qquad (24)$$

where u^s_b is the beam surface longitudinal displacement, which is related to the beam surface strain by:

$$\varepsilon^s_b = \frac{\partial u^s_b}{\partial x} \tag{25}$$

Therefore,

$$\frac{\partial^2 y}{\partial x^2} = -\frac{2}{t_b}\varepsilon^s_b \tag{26}$$

Thus, a fourth order partial differential equation in terms of the surface strain of a Bernoulli-Euler beam can be obtained by differentiating both sides of equation (26) twice with respect to x, substituting the result into equation (22), differentiating the resulting equation twice with respect to x, and substituting equation (26) in the result to give:

$$E_b\frac{t_b^2}{12}\frac{\partial^4 \varepsilon^s_b}{\partial x^4} - \rho_b\frac{\partial^2 \varepsilon^s_b}{\partial t^2} = 0 \tag{27}$$

For single frequency excitation:

$$\frac{\partial^2 \varepsilon^s_b}{\partial t^2} = -\omega^2\varepsilon^s_b \tag{28}$$

and equation (27) becomes:

$$E_b \frac{t_b^2}{12} \frac{\partial^4 \varepsilon_b^s}{\partial x^4} + \rho_b \omega^2 \varepsilon_b^s = 0 \qquad (29)$$

The beam system shown can be split into three separate beams and if the stiffness and weight contributions from the actuators are ignored, then it is possible to describe the dynamic system with three separate differential equations and use appropriate boundary conditions at the ends of each beam to obtain the required solutions. Thus the equations in terms of ε^s_{b1}, ε^s_{b2}, and ε^s_{b3}, are respectively:

$$E_b \frac{t_b^2}{12} \frac{\partial^4 \varepsilon_{b1}^s}{\partial x^4} + \rho_b \omega^2 \varepsilon_{b1}^s = 0 \qquad (30)$$

$$E_b \frac{t_b^2}{12} \frac{\partial^4 \varepsilon_{b2}^s}{\partial x^4} + \rho_b \omega^2 \varepsilon_{b2}^s = 0 \qquad (31)$$

$$E_b \frac{t_b^2}{12} \frac{\partial^4 \varepsilon_{b3}^s}{\partial x^4} + \rho_b \omega^2 \varepsilon_{b3}^s = 0 \qquad (32)$$

The solutions for ε^s_{b1}, ε^s_{b2}, and ε^s_{b3} are respectively:

$$\varepsilon^s_{b1}(x,\omega) = a_1 e^{jkx} + a_2 e^{-jkx} + a_3 e^{kx} + a_4 e^{-kx} \quad \text{for } x < x_1 \tag{33}$$

$$\varepsilon^s_{b2}(x,\omega) = a_5 e^{jkx} + a_6 e^{-jkx} + a_7 e^{kx} + a_8 e^{-kx} \quad \text{for } x_1 \le x \le x_2 \tag{34}$$

$$\varepsilon^s_{b3}(x,\omega) = a_9 e^{jkx} + a_{10} e^{-jkx} + a_{11} e^{kx} + a_{12} e^{-kx} \quad \text{for } x > x_2 \tag{35}$$

where the wave number k is defined as:

$$k = \left(\frac{12\rho_b \omega^2}{E_b t_b^2} \right)^{1/4} \tag{36}$$

The boundary conditions in terms of surface strains can be derived from boundary conditions in terms of vertical displacements. From equation (26) we can derive the following relationships:

$$\text{displacement} = y = -\frac{2}{t_b}\int\int \varepsilon_b^s dx dx \tag{37}$$

$$\text{angular displacement} = \theta = -\frac{2}{t_b}\int \varepsilon_b^s dx \tag{38}$$

$$\text{curvature} = R = -\frac{2}{t_b}\varepsilon_b^s \tag{39}$$

$$\text{shear force} = S = -\frac{2E_b}{t_b}\frac{\partial \varepsilon_b^s}{\partial x} \tag{40}$$

For the three sub-beams outlined in Figure 5, a total of ten (10) boundary conditions can be derived.

There are two full boundary conditions at $x=0$ and two at $x=L_x$, which are that there is no strain nor any displacement at these locations.

There are four (4) partial boundary conditions at $x=x_1$ and four at $x=x_2$, which are that there is continuity in strain, slope, curvature, and shear.

The boundary conditions are as follows:

At $x=0$:

$$\varepsilon^s_{b1}|_{x=0} = 0 \tag{41}$$

$$\iint \varepsilon^s_{b1}|_{x=0} = 0 \tag{42}$$

At $x=x_1$:

$$\iint \varepsilon^s_{b1} dx dx|_{x=x_1} - \iint \varepsilon^s_{b2} dx dx|_{x=x_1} = 0 \tag{43}$$

$$\int \varepsilon^s_{b1} dx|_{x=x_1} - \int \varepsilon^s_{b2} dx|_{x=x_1} = 0 \tag{44}$$

$$\varepsilon^s_{b1}|_{x=x_1} - \varepsilon^s_{b2}|_{x=x_1} = \varepsilon^s_a \tag{45}$$

$$\frac{\partial \varepsilon^s_{b1}}{\partial x}|_{x=x_1} - \frac{\partial \varepsilon^s_{b2}}{\partial x}|_{x=x_1} = 0 \tag{46}$$

At $x=x_2$:

$$\iint \varepsilon^s_{b2} dx dx|_{x=x_2} - \iint \varepsilon^s_{b3} dx dx|_{x=x_2} = 0 \quad (47)$$

$$\int \varepsilon^s_{b2} dx|_{x=x_2} - \int \varepsilon^s_{b3} dx|_{x=x_2} = 0 \quad (48)$$

$$\varepsilon^s_{b2}|_{x=x_2} - \varepsilon^s_{b3}|_{x=x_2} = -\varepsilon^s_a \quad (49)$$

$$\frac{\partial \varepsilon^s_{b2}}{\partial x}|_{x=x_2} - \frac{\partial \varepsilon^s_{b3}}{\partial x}|_{x=x_2} = 0 \quad (50)$$

At $x=L_x$:

$$\varepsilon^s_{b3}|_{x=L_x} = 0 \quad (51)$$

$$\iint e^s_{b3}|_{x=L_x} = 0 \quad (52)$$

The boundary conditions, equations (41) to (42), can be used together with equations (33) to (35) to solve for the unknown coefficients a_1 to a_{12}. These can then be substituted back into equations (33) to (35) to calculate the strain at any location x in any of the three sub-beams. This procedure is well documented by Pan *et al.* (1992) and will not be repeated here.

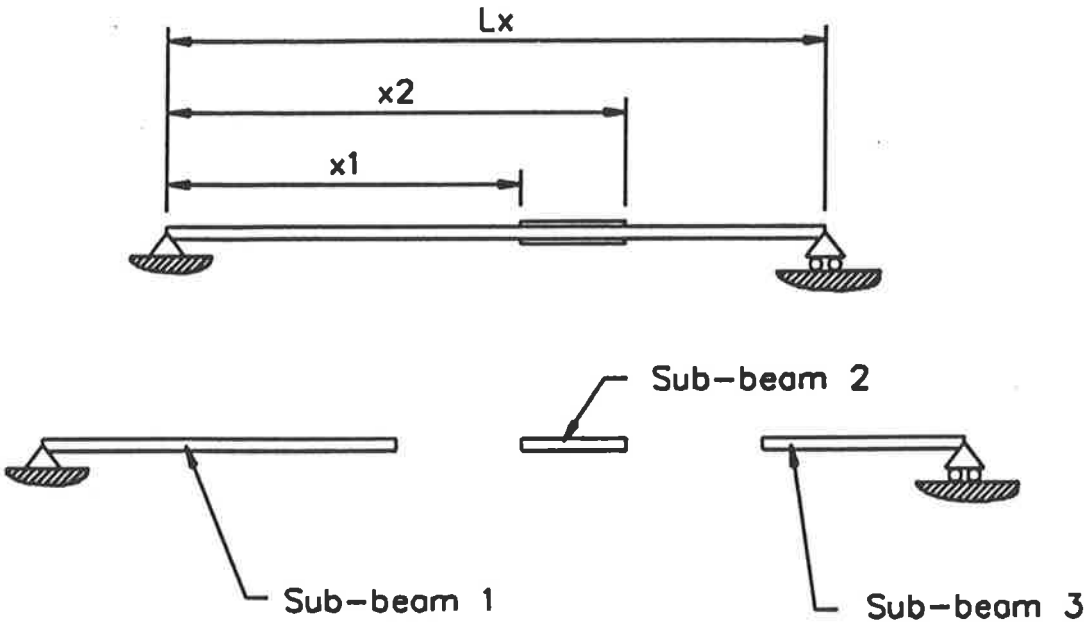

Figure 5. Beam and sub-beam system

3.3 Comparison of experimental and analytical results for a thin beam

3.3.1 Experimental set-up and computation of data

The overall dimensions of the instrumented simply supported beam (see Figures 6 and 7) are as shown in Table 1. Strain gauges were mounted above and beneath the actuator (see Figure 8) in an attempt to quantify the effects of the free edge of the actuator/beam interface.

Beam length	L_x (mm)	345
Beam width	b_b (mm)	40
Beam thickness	t_b (mm)	1.98
First actuator edge location	x_1 (mm)	173
Second actuator edge location	x_2 (mm)	206
Actuator length	L_c (mm)	33
Actuator width	b_c (mm)	40
Actuator thickness	t_c (mm)	0.2

Table 1. Beam and actuator dimensions

Material constants for the PZT G-1195 material actuator and mild steel beam system are as listed in Table 2. Damping is represented by using the complex form of Young's modulus ($E(1+j\eta)$) for both materials.

Actuator density	ρ_c (kg/m^3)	7275
Actuator Young's modulus	E_c (Pa)	63 x 10^9
Piezoelectric constant	d_{31} (m/V)	1.9 x 10^{-10}
Actuator loss factor	η_c	0.0125
Beam density	ρ_b (kg/m^3)	7860
Beam Young's modulus	E_b (Pa)	200 x 10^9
Beam loss factor	η_b	0.01

Table 2. Actuator and beam material parameters

From the various theoretical models outlined in Section 3.1, and the physical dimensions and material values for this particular test beam, it is possible to determine ε^s_a from equations (8) to (18) corresponding to each of the theoretical models. Values of Poisson's ratio for both beam and piezoelectric actuators were taken as zero in the models which considered plate equations to enable this comparison. These results are shown in Table 3.

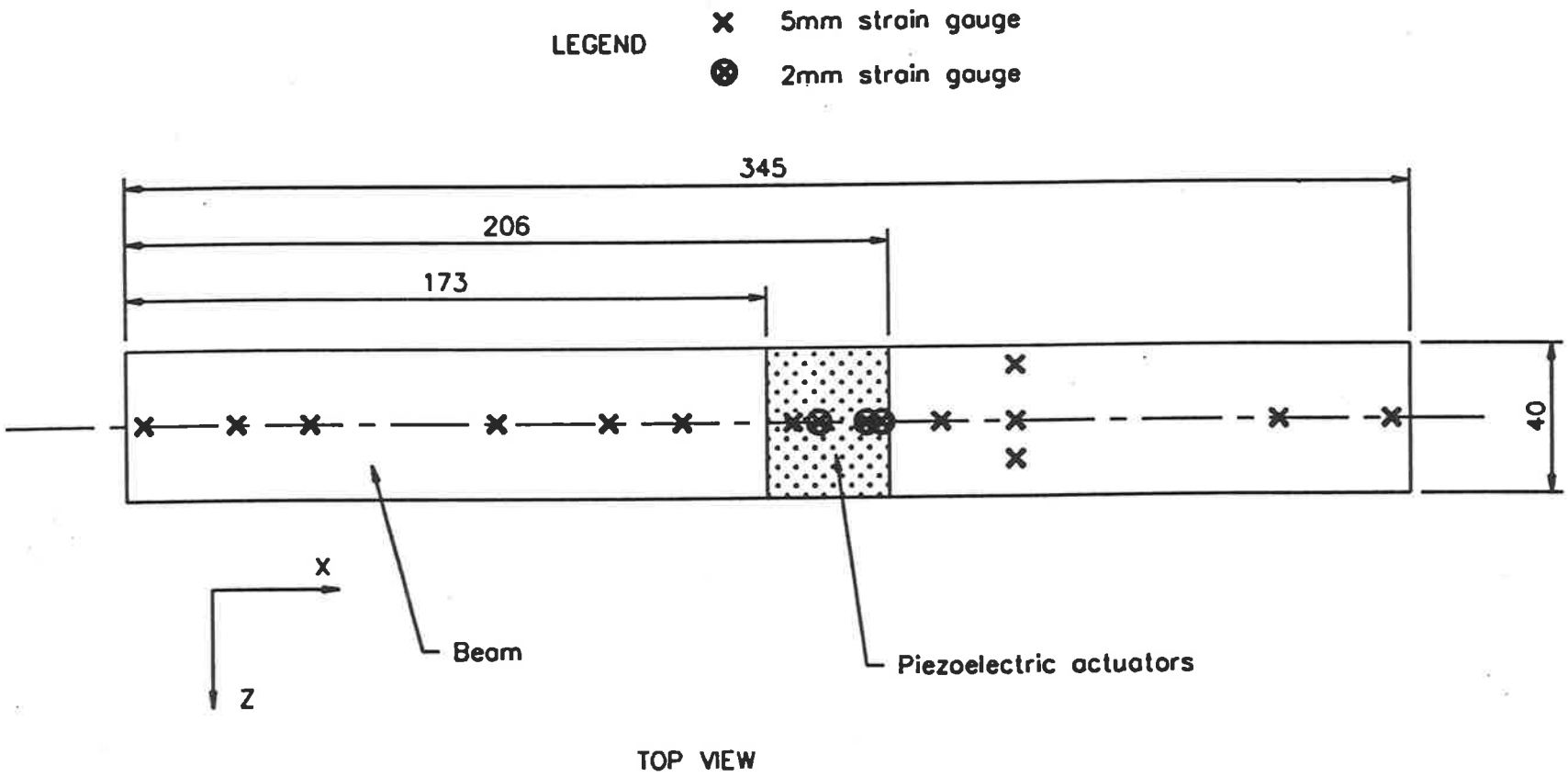

Figure 6. Overall beam measurements

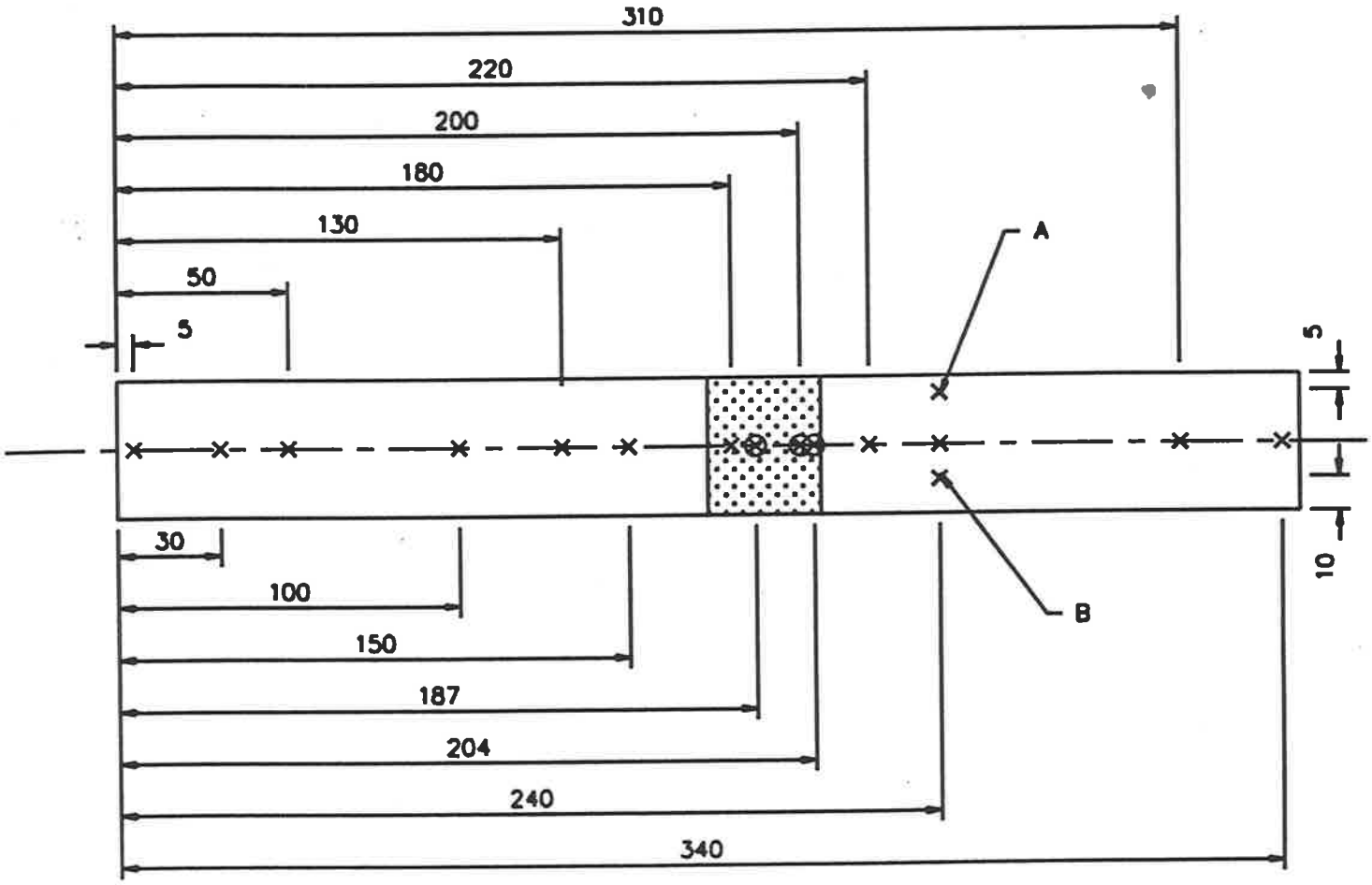

Figure 7. Strain gauge locations

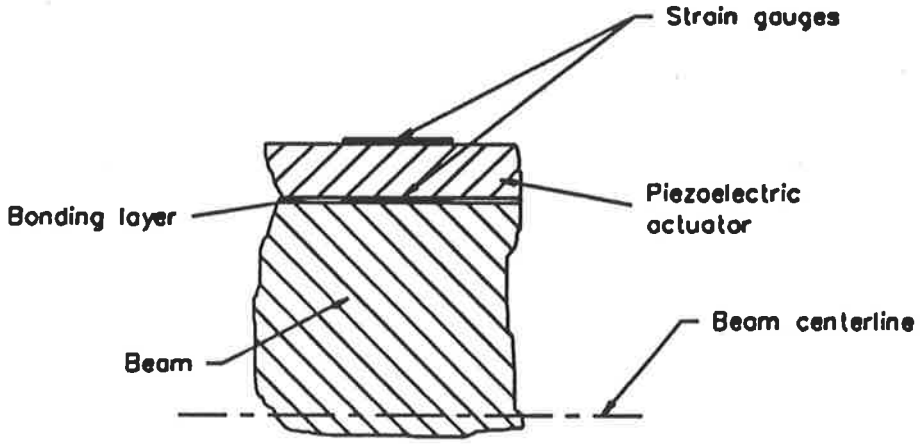

Figure 8. Cross section through experimental instrumented beam

MODELS	ε^s_a
Crawley and de Luis (1987)	0.1603 Λ
Crawley and Anderson (1990)	0.1706 Λ
Kim and Jones (1991)	0.1706 Λ
Clark et al. (1991)	0.1642 Λ
Dimitriadis and Fuller (1991)	0.1642 Λ
Pan et al. (1992)	Λ

Table 3. Values of ε^s_a corresponding to each theoretical model for the test beam

The dynamic model postulated here is compared to a modified version of the model proposed by Clark *et al.*, (1991). The beam vertical displacement has been converted into beam surface strain by equation (26). The converted results of the Clark *et al.* (1990) model can be expressed as:

$$\varepsilon_b^s = C_o \sum_{n=1}^{\infty} \frac{n^3}{(\omega_n^2 - \omega^2)} \left[\cos\frac{n\pi x_1}{L_x} - \cos\frac{n\pi x_2}{L_x}\right] \sin\frac{n\pi x}{L_x} \qquad \textbf{(53)}$$

where $\varepsilon^s{}_b$ is the beam surface strain at any point x, and:

$$\omega_n^2 = \frac{E_b t_b^2}{12\rho_b}\left(\frac{\pi n}{L_x}\right)^4 \qquad \textbf{(54)}$$

and

$$C_o = -E_b \frac{P}{6(1-P)} t_b^2 \qquad \textbf{(55)}$$

where P is defined by equation (13).

The value of the interface strain $\varepsilon^s{}_a$ in the corrected model presented in this comparison of results is based on the interface strain value obtained by Crawley and Anderson (1990). The results obtained from the Clark *et al.* (1990) model are based directly upon equations from their paper, and thus as mentioned previously due to their assumed stress distribution, their results underestimate the applied strain distribution by around 4% or equivalently are in error by 0.35 dB.

The experimental arrangement used for the tests was as shown in Figure 9. The HP3562A frequency analyser was used in a slow swept frequency mode which was preferred as it closely matched the model condition of single frequency excitation (see equation (28)). Furthermore, the feedback control capability of this analyser was also used as it enabled the control of the input voltage using the output strain value. This feature enabled the extension of the dynamic range to well beyond 80 dB, while still providing adequate signal to noise ratio. All presented data are transfer functions, between resultant strain and input actuator voltage in dB (re 1 strain/V), where the sinusoidal voltage applied to the actuator was less than 100 V rms, which is shown to be well within the linear range of the piezoelectric actuator (see Section 5.2).

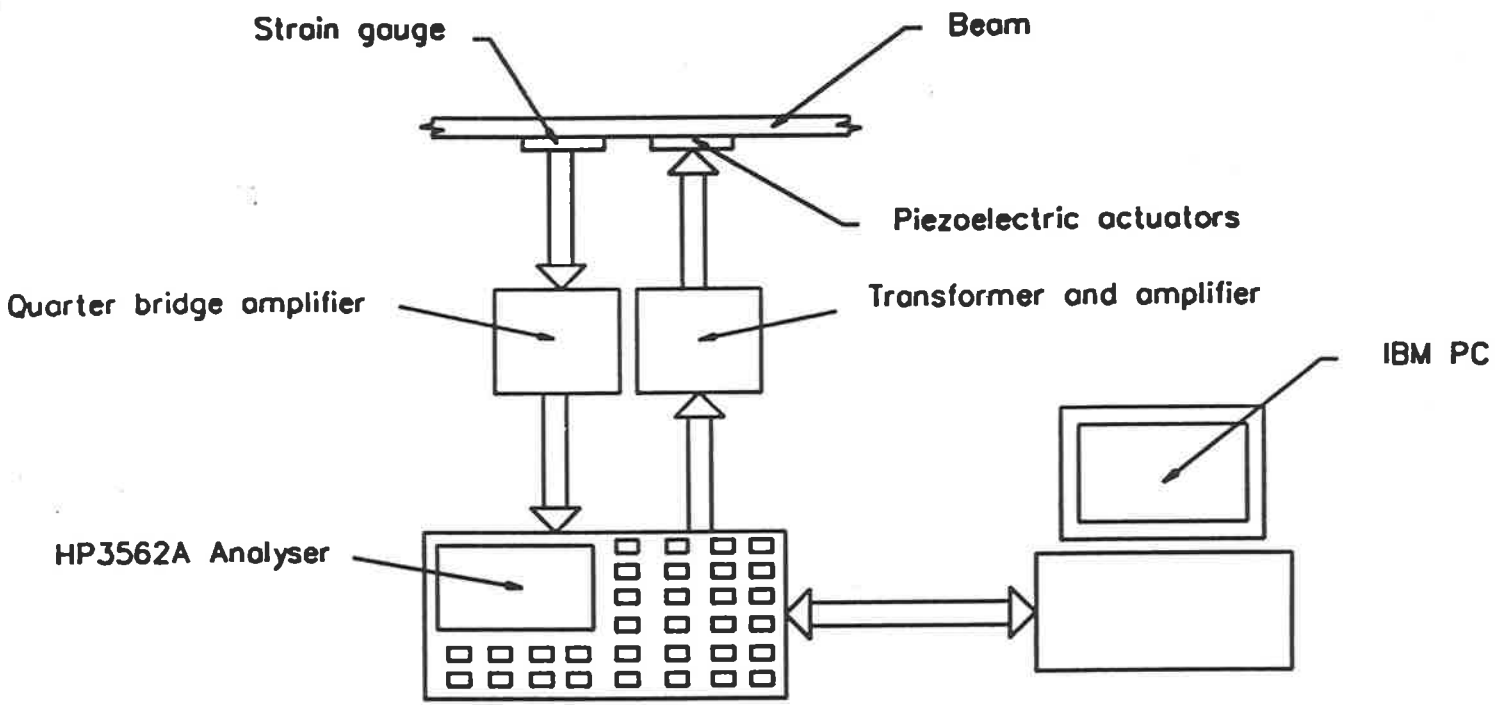

Figure 9. Experimental set-up

3.3.2 Results and discussion

Figure 10 shows the strain values recorded at three different positions across the beam at x=240 mm. The uniformity of these results, from one position to another show that the beam is indeed behaving as a beam, rather than as a narrow plate. Further, the results demonstrate the repeatability of the experiment, as these measurements where not taken concurrently.

There is also very good agreement between both the Clark *et al.* (1990) model, the model postulated here and the experimental data at all measurement points (see Figures 11, 12, and 13). Indeed, there is little if no difference between the dynamic models. The small differences between the models can be attributed to the fact that only the first 100 modes are used to calculate the resulting strain for the Clark *et al.* (1990) model, and not an infinite sum as in equation (53). It must also be pointed out that the stiffness or weight contribution of the piezoelectric actuator are not considered in either models. If the stiffness contribution was included, in a similar fashion to Pan *et al.*, (1992), by including the actuator stiffness within the wave number for the beam portion containing the actuator, the effect is negligible. Thus, it may be concluded that piezoelectric stiffness and inertia effects can be disregarded.

Both analytical models accurately predict the resonant mode shapes and resonance frequencies. However at non-resonant frequencies corresponding to beam forced response, there are discrepancies between measured and predicted levels, with the analytical models consistently over predicting the measured response levels. However, coincidently at some

discrete frequencies, the theoretical models and experimental results do agree (eg. 420 Hz). The resonant mode response shapes calculated from the models, and shown in Figures 14 to 16, agree well with the experimental results. From the above observations, it is apparent that the models generally over predict the beam response at non resonance frequencies, although at some frequencies (420 Hz, for example) the measured and predicted strain levels agree, and hence the non resonant response is well predicted (Figure 18).

The comparison of the resonant and non resonant response (Figures 16 and 17) of the piezoelectric actuator is very enlightening. At a beam resonance frequency, the strain on the top surface of the actuator is just an amplification of the strain at the actuator/beam interface. Indeed, from purely geometrical considerations, the amplification is approximately 2 dB. (ie. $20\ log10((t_b+2t_c)/t_b)$). This agrees very well with experimental results (Figure 16). Thus the assumption that the strain distribution is linear across the actuator/beam interface, over the whole actuator/beam sub section, is validated. The actuator/beam force transfer mechanism in this case can be thought of being either a distributed applied strain $\varepsilon^s{}_a$ or a pair of applied line moments M_z.

On the other hand, the measured non resonant response does not support this assumption. Indeed, the strain distribution across the top of the piezoelectric actuator (Figure 17) is reminiscent of the results derived by Crawley and de Luis, (1987). Away from resonance the impedance of the beam is high, and the actuator/beam force transfer mechanism changes. In this case the transfer mechanism is more likely to be the shear lag mechanism described by Crawley and de Luis (1987), and since experimentally measured strains are

smaller than predicted strains, this mechanism is obviously less efficient than the distributed applied strain or line moment mechanisms. This conclusion is supported by the results given in Figures 18 and 19 which show that:

- Away from resonances, the force transfer mechanism becomes less efficient
- Away from the actuator edge, the shear lag effect becomes less pronounced

Equation (7) defines the moment in the beam at any location beneath the actuator, assuming that the actuator is inducing pure bending in the beam. This assumption implies that the strain at the actuator/beam interface is uniform over the whole actuator/beam sub section. However, at the beam surface just prior to the actuator edge the applied strain will in practice tend to zero (see Figure 20), and this is true no matter what length the actuator might be (even if it is the entire length of the beam). Thus in the limit, there will be no applied strain right at the very edge of the actuator-beam interface. However, due to the stress free edge condition somewhere on the free edge, the strain must be Λ (by equation (5) setting $\sigma_c=0$, $\varepsilon_c=\Lambda$). This rapid change in applied strain results in a large increase in shear stress at the actuator/beam interface near the edge of the actuator, a phenomenon commonly referred to as shear lag (Crawley and de Luis, 1987). For stiff bonding layers or perfectly bonded actuators, the increased shear will effectively occur just prior to the edge of the crystal-beam interface. The rate of change of strain is less for less stiff bonding layers (Crawley and de Luis, 1987) resulting in a smaller shear stress peak at the edge of the actuator but with a finite shear stress extending further in towards the centre of the actuator. This shear lag effect acts to reduce the accuracy of the predicted beam response obtained using the ideal excitation model consisting of the two counteracting line moments, or the uniformly distributed applied strain.

Although the shear lag effects were recognised in the Crawley and de Luis model (1987), lack of other considerations (such as bending of the actuators) limit its usefulness. Nevertheless, this model is valuable because of its ability to give some idea of the force transfer mechanism in the near field.

A second inaccuracy, in the traditional modelling approach of assumed pure bending, is that for pure bending, the moment must be produced by end tensions and compressions having magnitudes in proportion to their distance from the neutral axis. Applying strains to the top and bottom surfaces of the beam can only approximate this ideal condition, resulting in further errors in beam response calculations.

The approximation of replacing the effect of the piezoelectric pair by a pair of counteracting line moments M_z or a uniformly distributed strain $\varepsilon^s{}_a$ gives accurate predictions of the beam response at resonant frequencies and at locations far from, and relatively close to, the free edge of the actuator. This would be justified by using a dynamic equivalent of the static Saint Venant's principle which states that any forces acting on a small portion of a body may be replaced by another statically equivalent system of forces acting on the same portion of a body, which produces significant changes within the local stress field, but has no significant effect at distances which are large compared to the dimension of the portion upon which the forces have been changed (Timoshenko and Goodier, 1951). Thus, the replacement of the action of the piezoelectric actuators by an equivalent line moment M_z or the uniformly distributed strain $\varepsilon^s{}_a$ is only valid at resonant frequencies. In this regime, the free edge condition of the piezoelectric actuator does not affect the associated strain field, and hence the assumptions made when

modelling M_z or ε^s_a are substantiated. But the replacement of the force transfer mechanism of the actuator by an equivalent mechanism at non resonant frequencies is not validated. In that regime, the stress field local to the free edge condition of the piezoelectric actuator means that the force transfer mechanism is markedly different, and hence M_z or ε^s_a are no longer equivalent force transfer mechanisms.

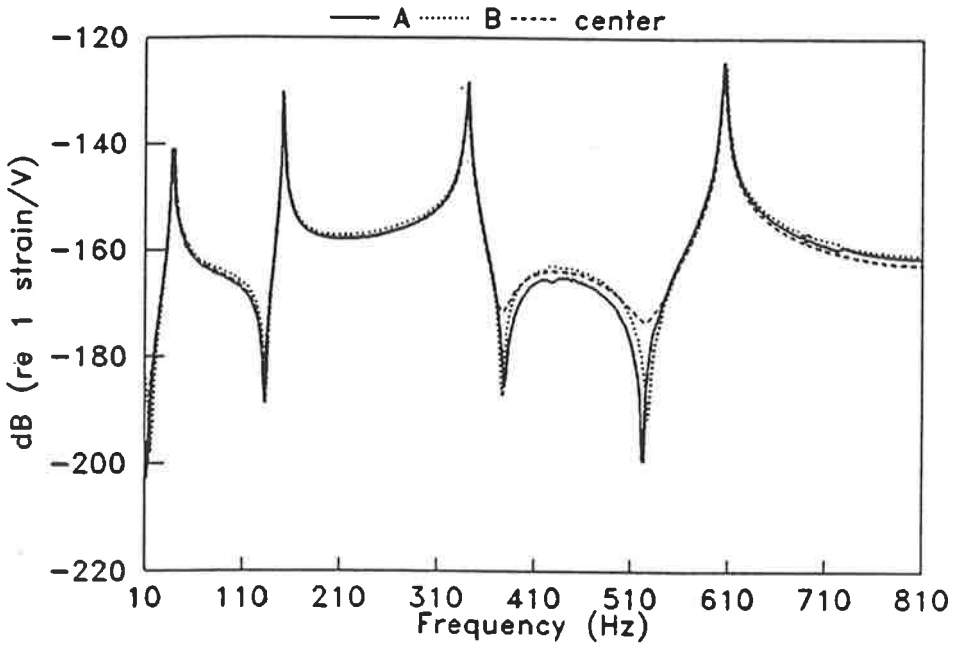

Figure 10. Strain transfer function at x=240 mm

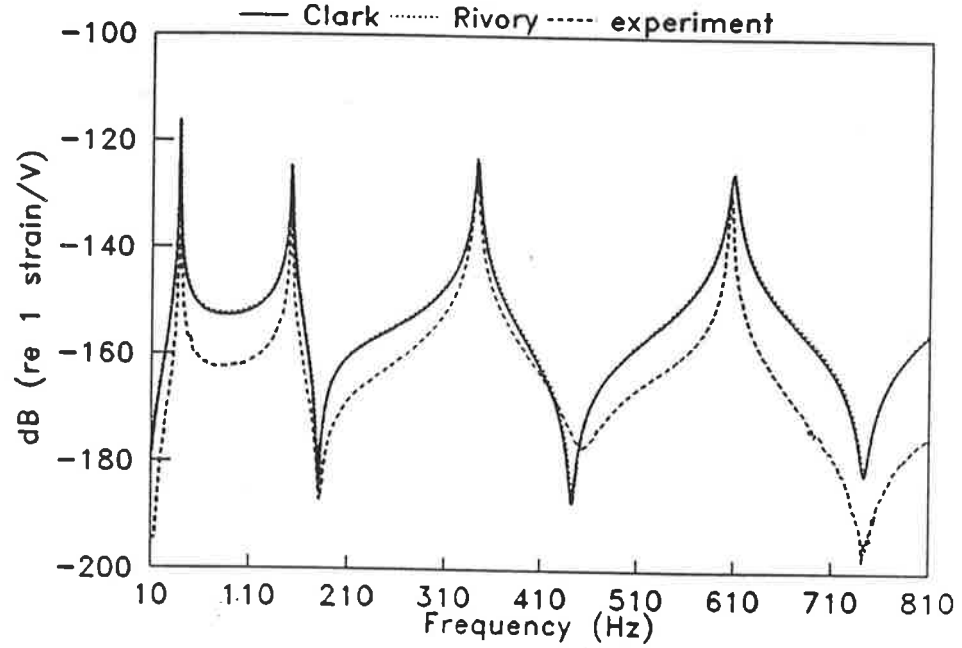

Figure 11. Comparison of theoretical models and experimental data at x=100 mm

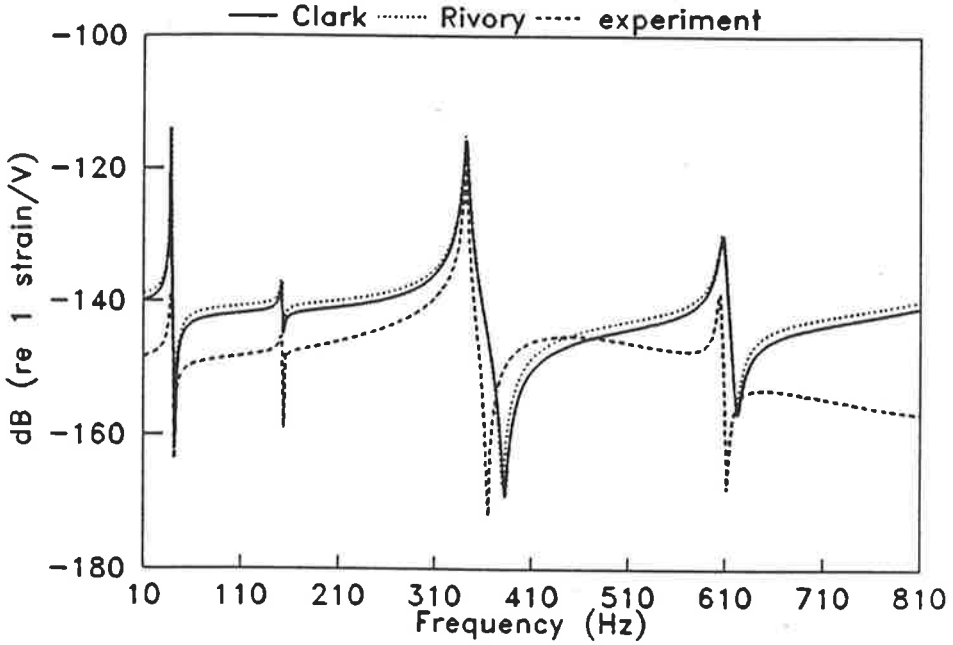

Figure 12. Comparison of models and experimental data at x=180 mm

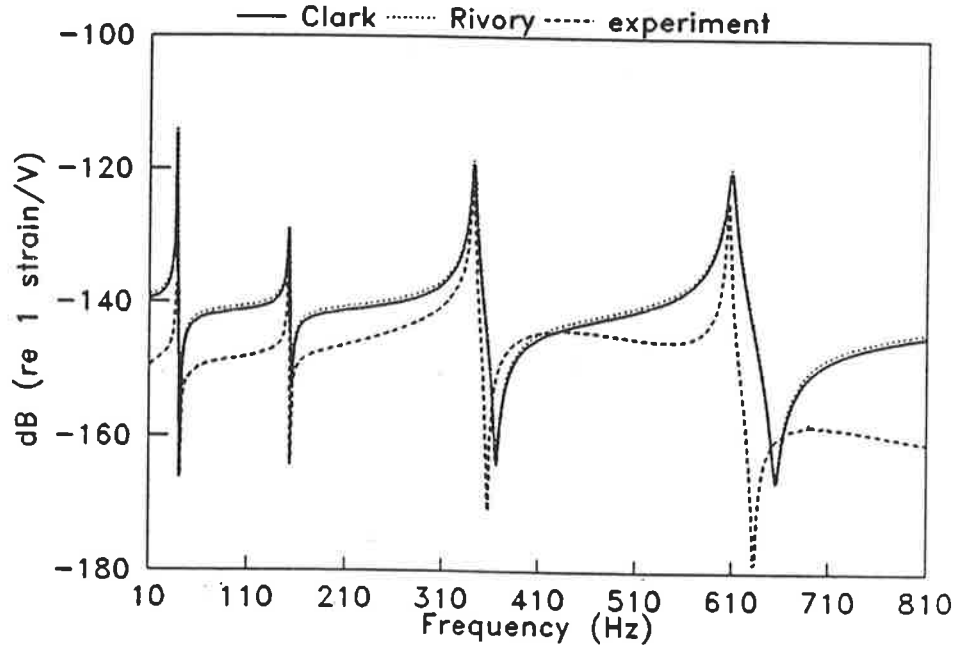

Figure 13. Comparison of theoretical models and experimental data at x=204 mm

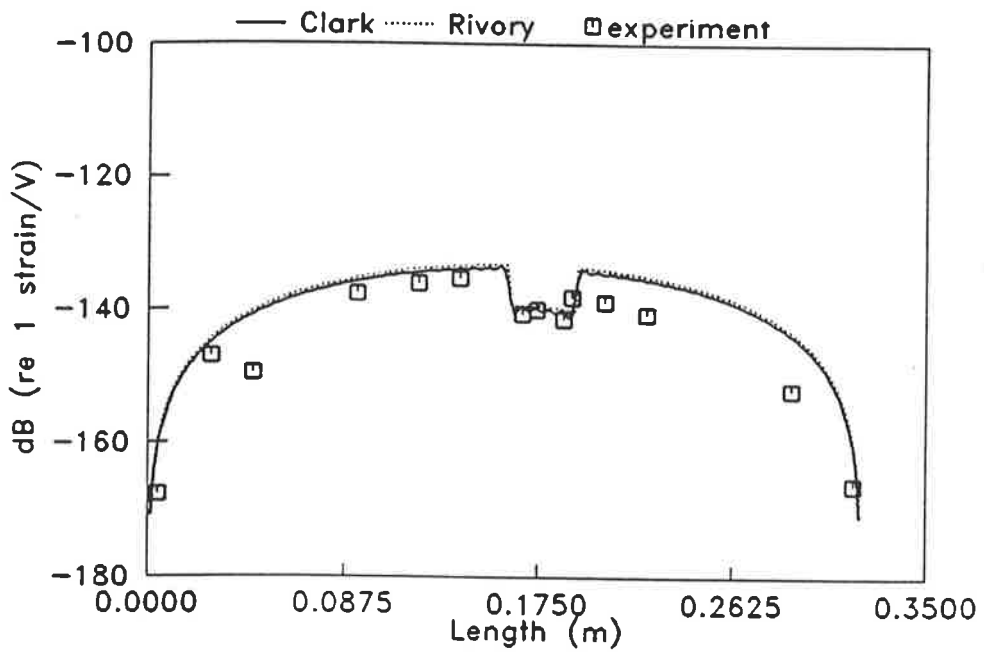

Figure 14. Comparison of theoretical models and experimental data, 40 Hz mode shape

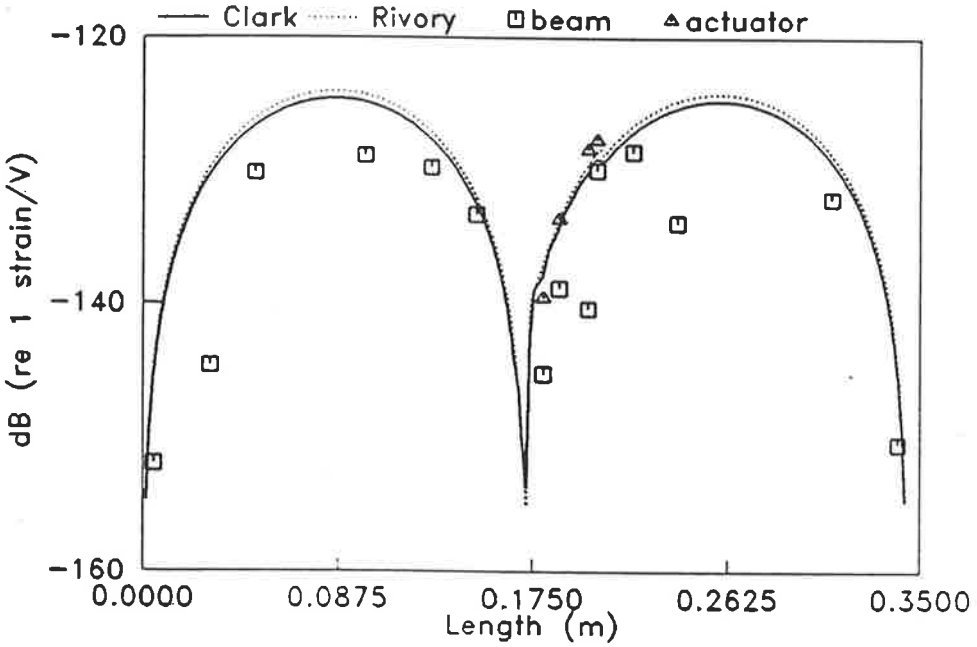

Figure 15. Comparison of theoretical models and experimental data, 152 Hz mode shape

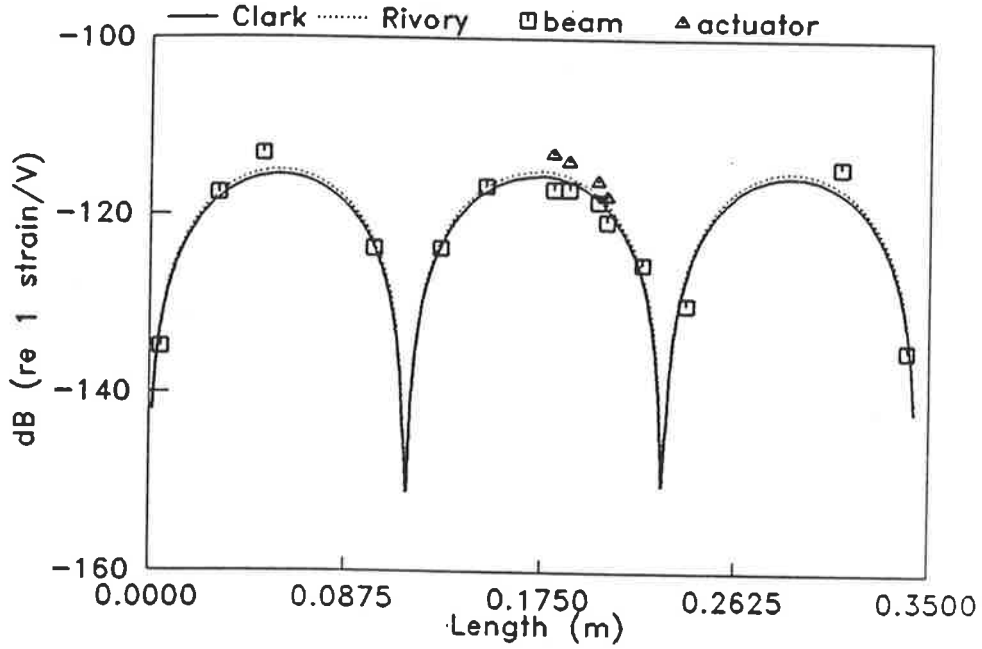

Figure 16. Comparison of theoretical models and experimental data, 342 Hz mode shape

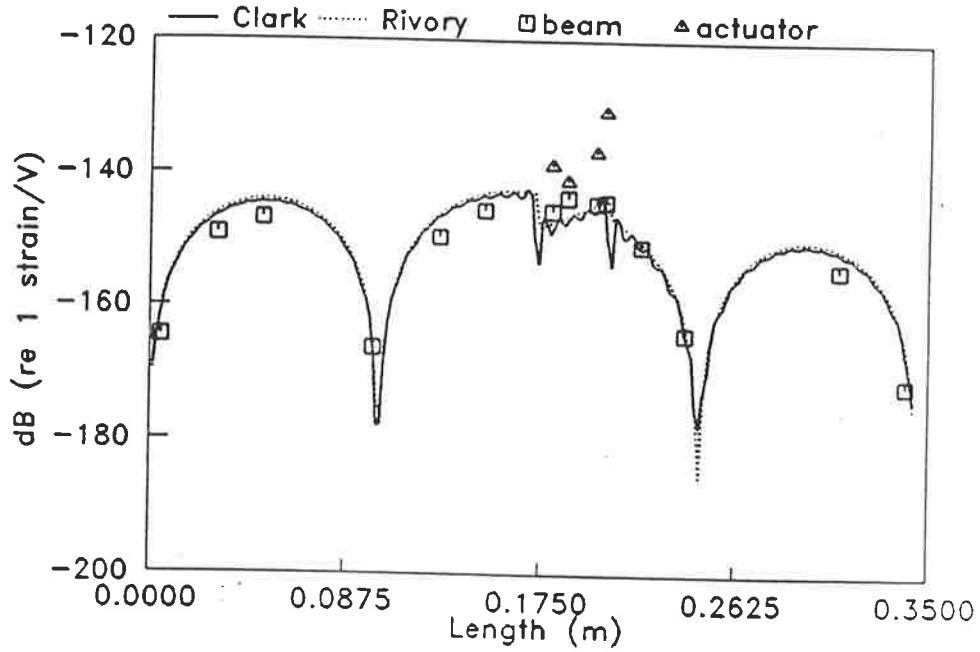

Figure 17. Comparison of theoretical models and experimental data, 420 Hz mode shape

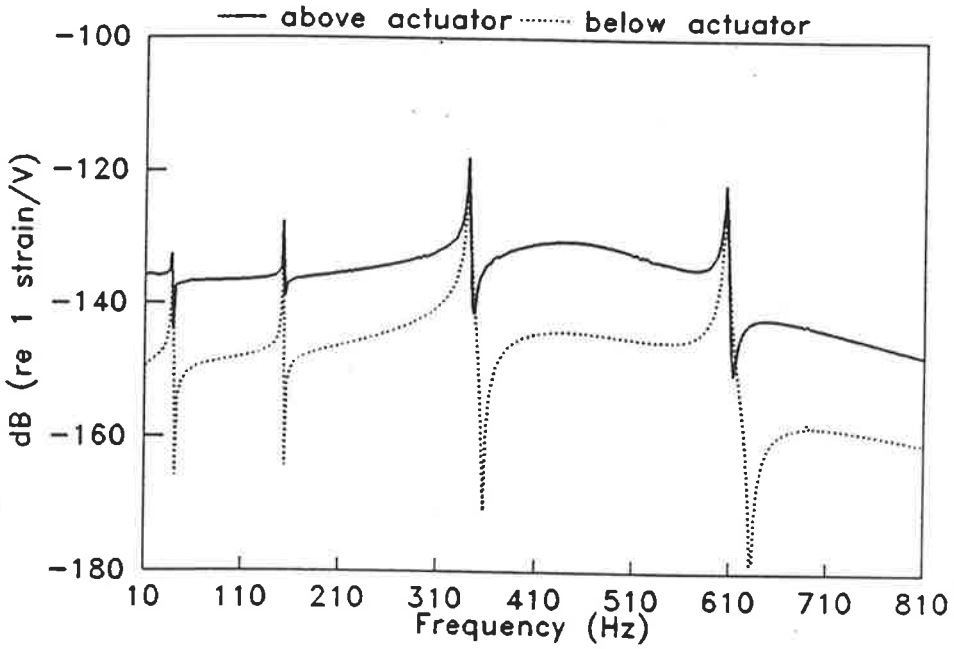

Figure 18. Comparison of measured strain above and below the actuator, at x=204 mm

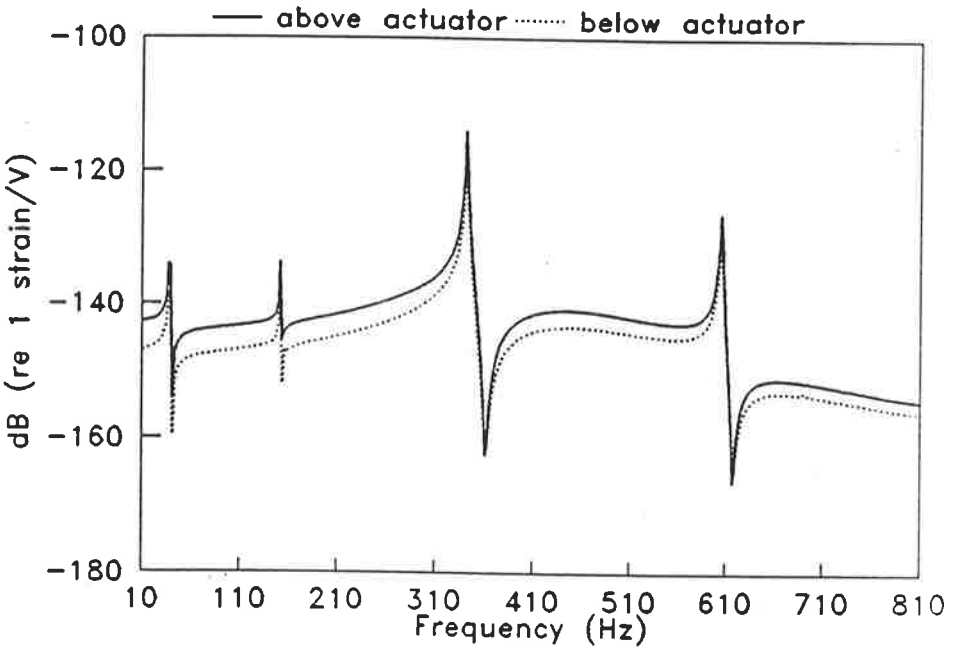

Figure 19. Comparison of strain above and below the actuator, at x=187 mm

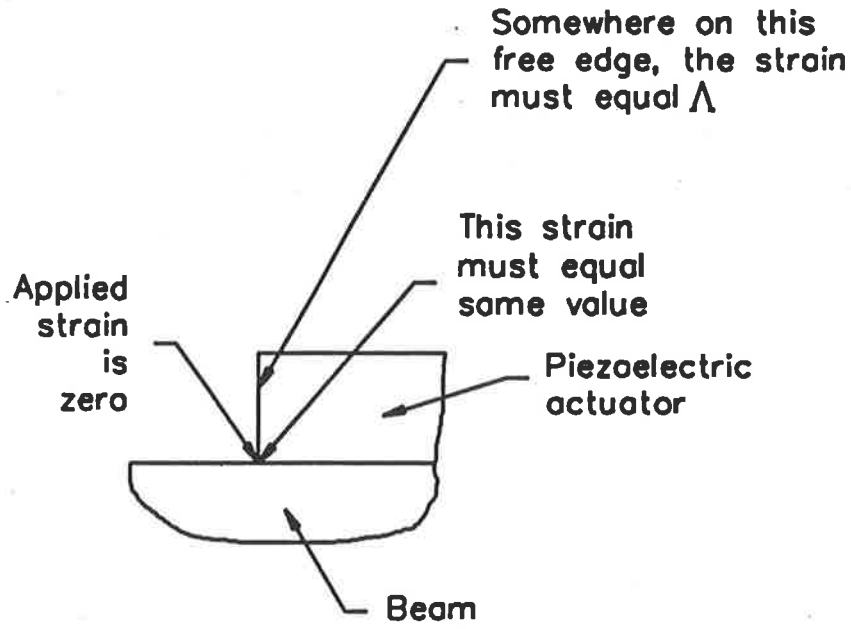

Figure 20. Near field strain singularity

3.4 Comparison of experimental and analytical results for a thick beam

3.4.1 Experimental set-up and computation of data

The overall dimensions of the instrumented simply supported aluminium beam (see Figure 21) are as shown in Table 4.

Material constants for the PZT G-1195 material actuator and beam system are as listed in Table 5. Damping is represented by using the complex form of Young's modulus ($E(1+j\eta)$) for both materials.

In this experiment with a thick beam, the beam and piezoelectric actuator widths are not the same (the beam width was 50 mm and the actuator width was 32 mm), yet only the expression from Crawley and Anderson (1990) (equation (10)) and the modified theory of Clark *et al.* (equations (19) to (21)) in Section 3.1 actually account for this.

5 mm and 2 mm strain gauges, at the locations listed in Table 3, were bonded to the top surface of the beam. Gauges of 2 mm length were located around the piezoelectric actuator in an effort to increase the measurement resolution at that location.

The experimental arrangement used for the tests was as shown in Figure 9. Again, the HP3562A frequency analyser was used in the swept frequency mode for the reasons stated in section 3.3.1

Beam length	L_x (mm)	3900
Beam width	b_b (mm)	50
Beam thickness	t_b (mm)	25.4
First actuator edge location	x_1 (mm)	2111
Second actuator edge location	x_2 (mm)	2150
Actuator length	L_c (mm)	39
Actuator width	b_c (mm)	32
Actuator thickness	t_c (mm)	0.2

Table 4. Beam and actuator dimensions

Actuator density	ρ_c (kg/m^3)	7275
Actuator Young's modulus	E_c (Pa)	63 x 10^9
Piezoelectric constant	d_{31} (m/V)	1.9 x 10^{-10}
Actuator loss factor	η_c	0.0125
Beam density	ρ_b (kg/m^3)	2710
Beam Young's modulus	E_b (Pa)	69 x 10^9
Beam loss factor	η_b	0.01

Table 5. Actuator and beam material parameters

STRAIN GAUGE X-COORDS (mm)	5 mm GAUGE	2 mm GAUGE	STRAIN GAUGE X-COORDS (mm)	5 mm GAUGE	2 mm GAUGE
100	Y		2116		Y
200	Y		2131		Y
350	Y		2136		Y
500	Y		2146		Y
900	Y		2150		Y
1280	Y		2170	Y	
1396	Y		2335	Y	
1426	Y		2365	Y	
1896	Y		2490	Y	
1926	Y		2740	Y	
2061	Y		2835	Y	
2111 A&B		Y	2865	Y	

Table 6. Strain gauge type and x-coordinates for the aluminium thick beam

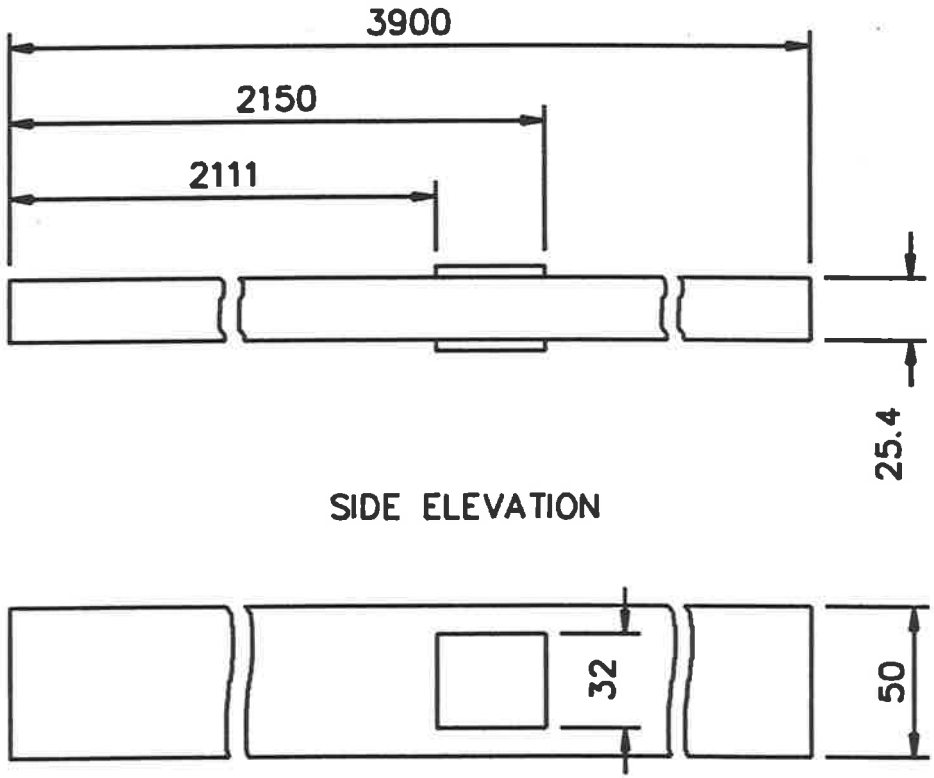

Figure 21. Instrumented aluminium beam

3.4.2 Results and discussion

Figure 22 shows the result from strain gauges A and B located at x = 2111 mm. Again despite the beam thickness, it appears that the beam is acting as a beam and not a thin plate, at least close to the actuator.

There is good agreement between the model and the experimental results close to the actuator (Figures 3 and 4). At regions far from the actuator, at low frequencies there is good agreement also; however, at higher frequencies, in between the resonance peaks, the agreement is poor (Figures 25 and 26). This is due to the presence of longitudinal waves which show that at higher frequencies, any small errors in actuator placement or response mean that the actuators are not truly 180° out phase which results in the excitation of longitudinal waves and their detection by the strain gauges.

It also appears that the resonance frequencies of the higher modes are over predicted by the model presented in this thesis. The model is based upon Bernoulli-Euler beam and hence does not account for shear deformation and rotary inertia. A model based upon the Timoshenko beam is required to predict these higher modes. Using a scheme presented by Craig, Jr. (1981), where the cross coupled shear deformation and rotary inertia terms are decoupled, it is possible to see the effects on the prediction of the resonance frequencies of the higher order modes (Table 7).

MODE NO	BERNOULLI EULER	TIMOSHENKO	EXPERIMENT
7	187.2	186.6	190
8	244.5	243.4	244
9	309.5	307.7	308
10	382.1	379.4	380
11	462.3	458.4	459
12	550.2	544.6	541
13	645.7	638.0	638
14	748.9	738.6	738

Table 4. Comparison of higher order modes, Bernoulli-Euler and Timoshenko beam models, and experimental results.

It is interesting to note that even for a beam as thick as the one used in this experiment, the shear deformation and rotary inertia effects are not significant until around the eighth mode.

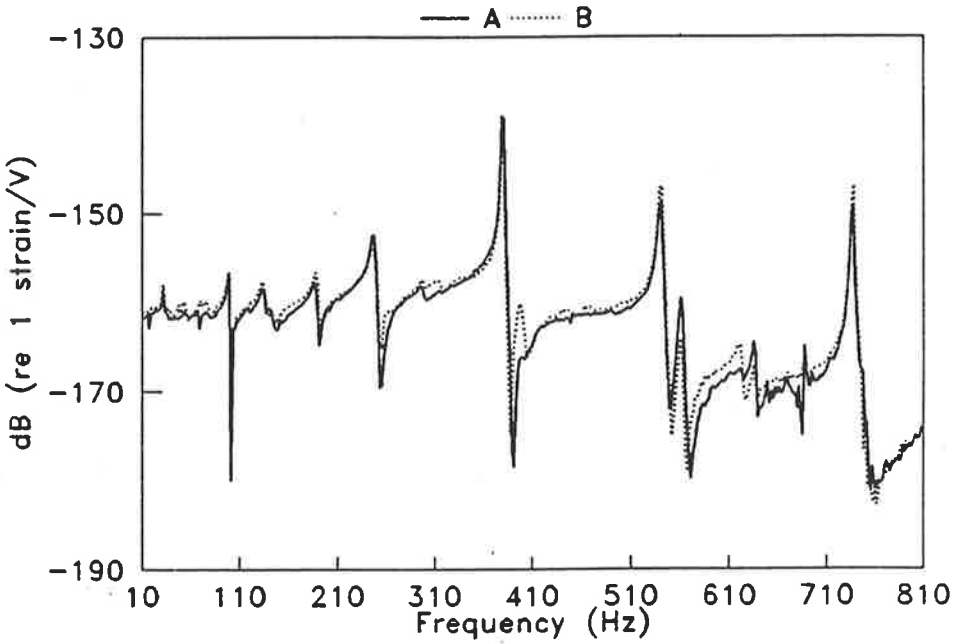

Figure 22. Comparison of strain at x=2111 mm

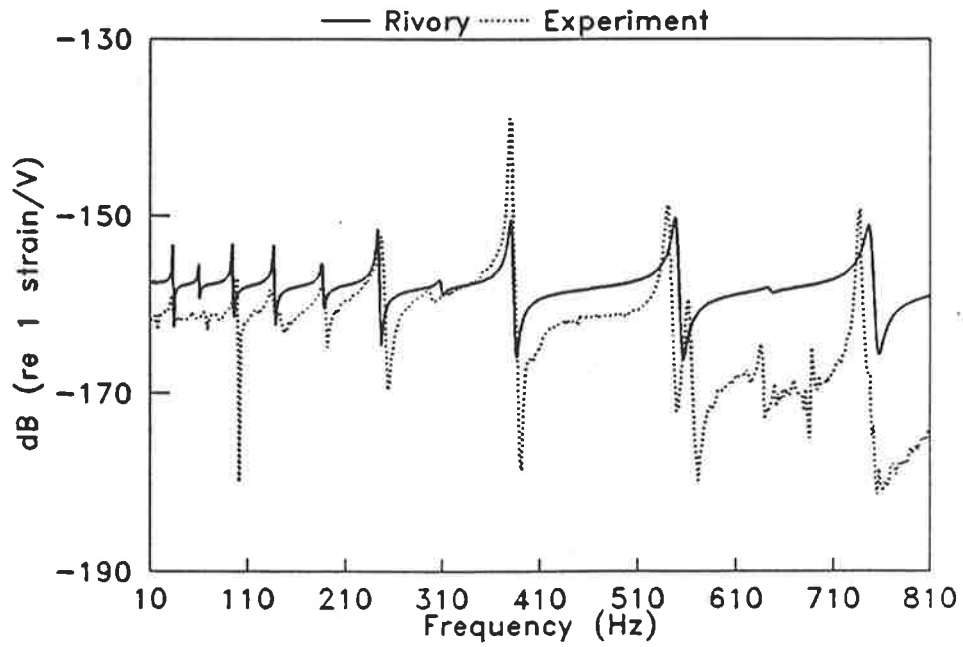

Figure 23. Comparison between model and experiment strain at x=2111 mm

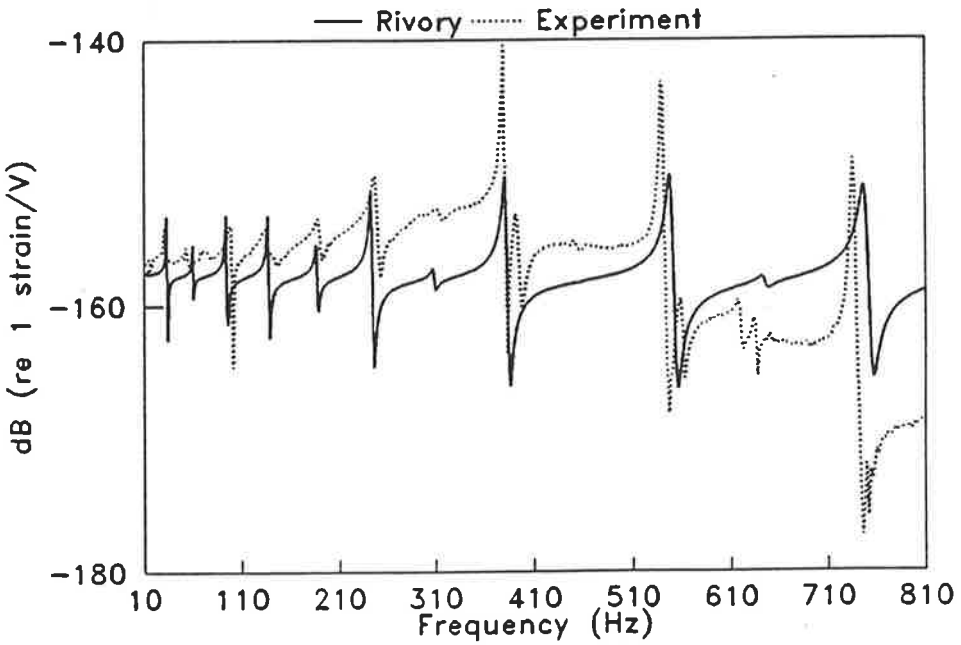

Figure 24. Comparison between model and experiment strain at x=2116 mm

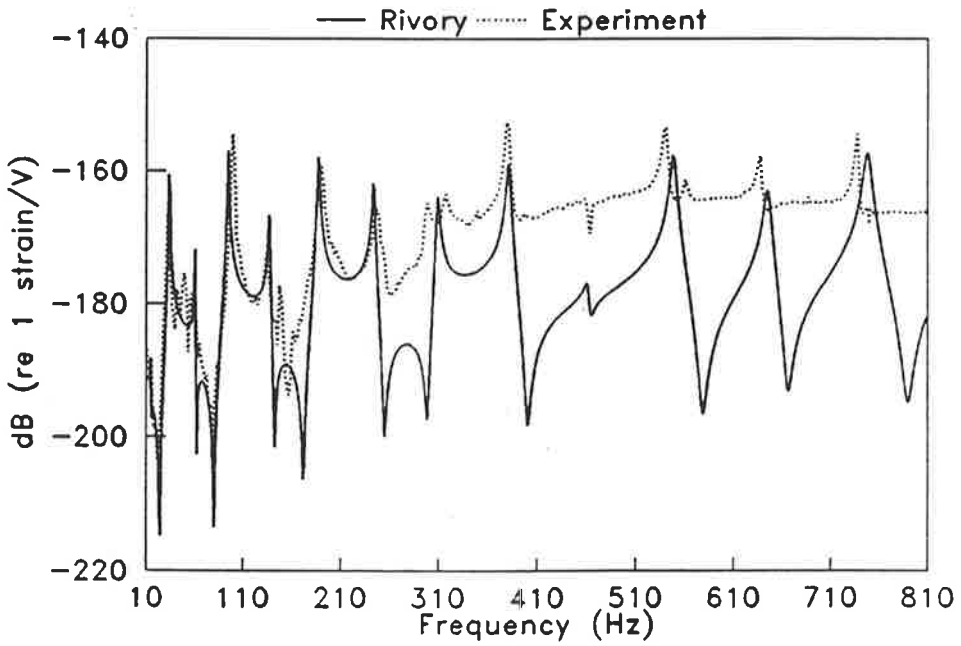

Figure 25. Comparison between model and experiment strain at x=1896 mm

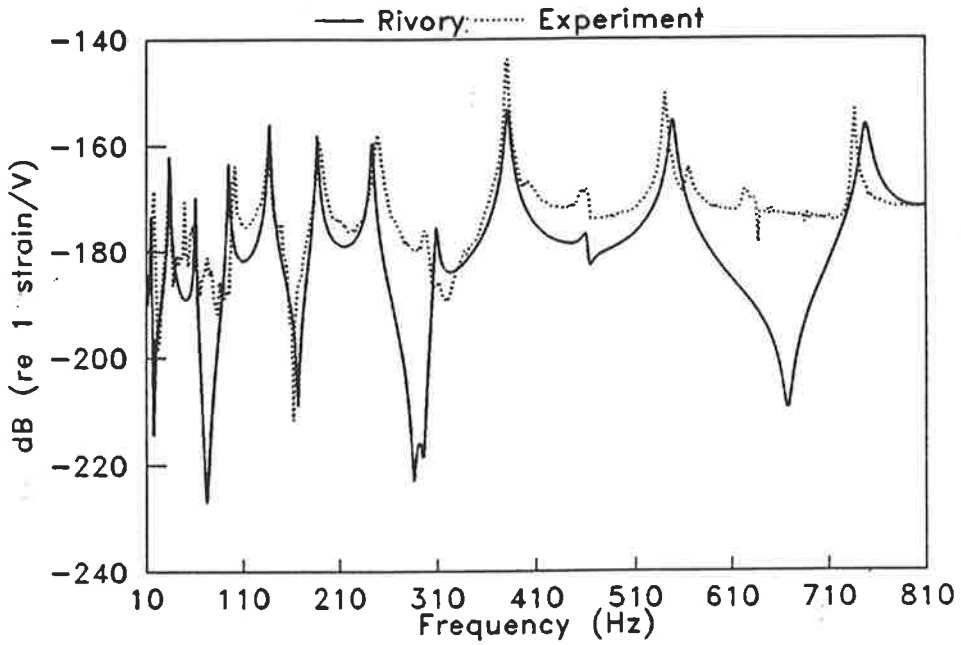

Figure 26. Comparison between model and experiment strain at x=900 mm

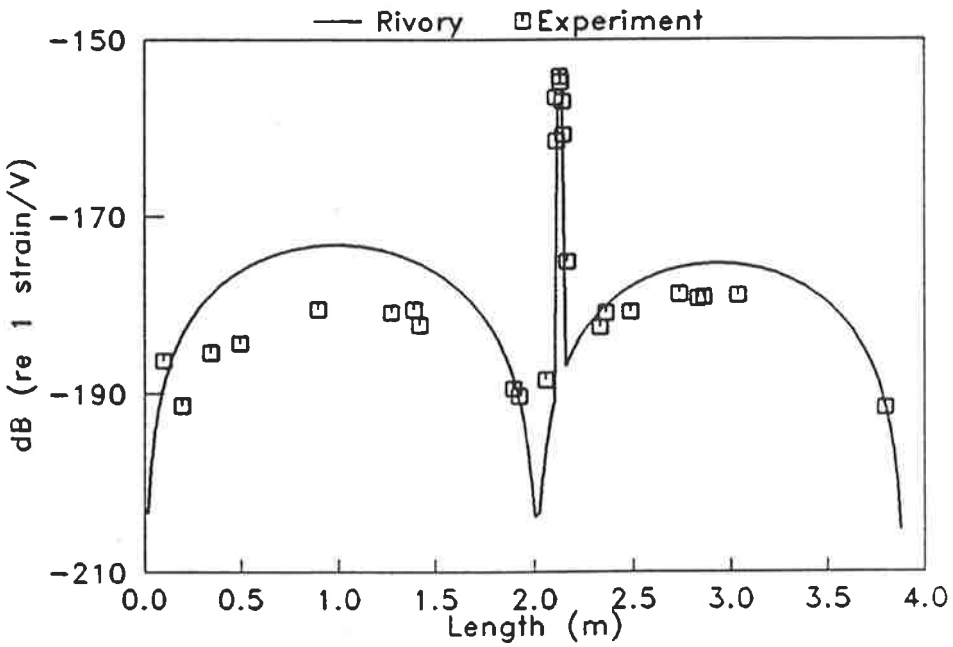

Figure 27. Strain mode shape for f=15 Hz (second mode)

At low frequencies, both resonant and non-resonant mode shapes are well predicted by the model. As well, for these frequencies, the dynamic response of the beam is also well predicted at points both close to and far from the piezoelectric actuator, see Figures 7, 8, and 9.

For higher order modes, and at frequencies between these higher order modes (Figure 10), the comparison between the model predictions and the experimental results is not as good. This is due to the presence of longitudinal waves in the experimental data and the frequency underestimation of the modal resonance frequencies modes by the model based on a Bernoulli-Euler beam.

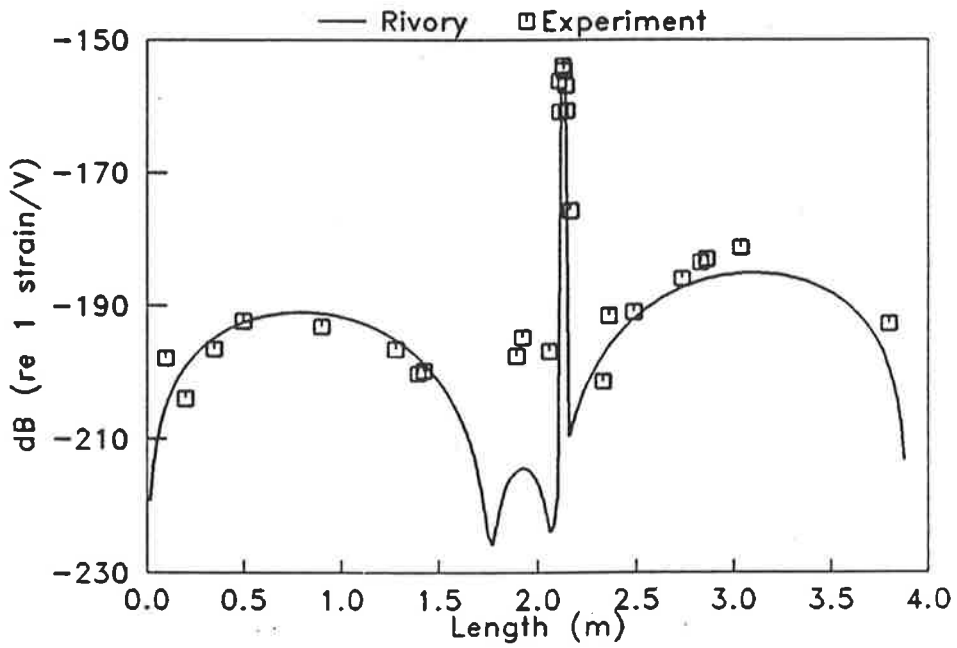

Figure 28. Strain mode shape for f=25 Hz

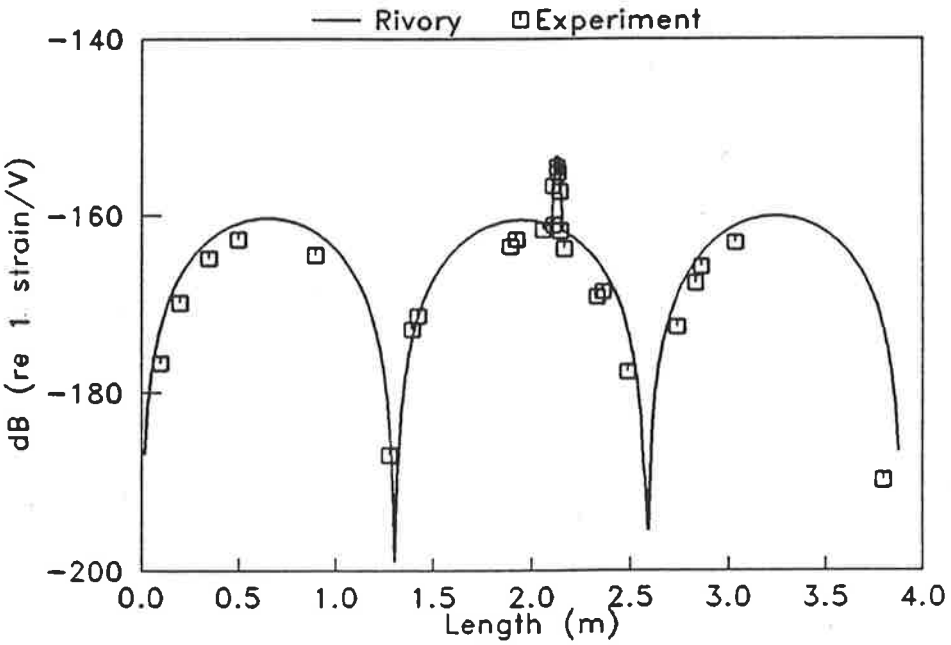

Figure 29. Strain mode shape for f=34 Hz (third mode)

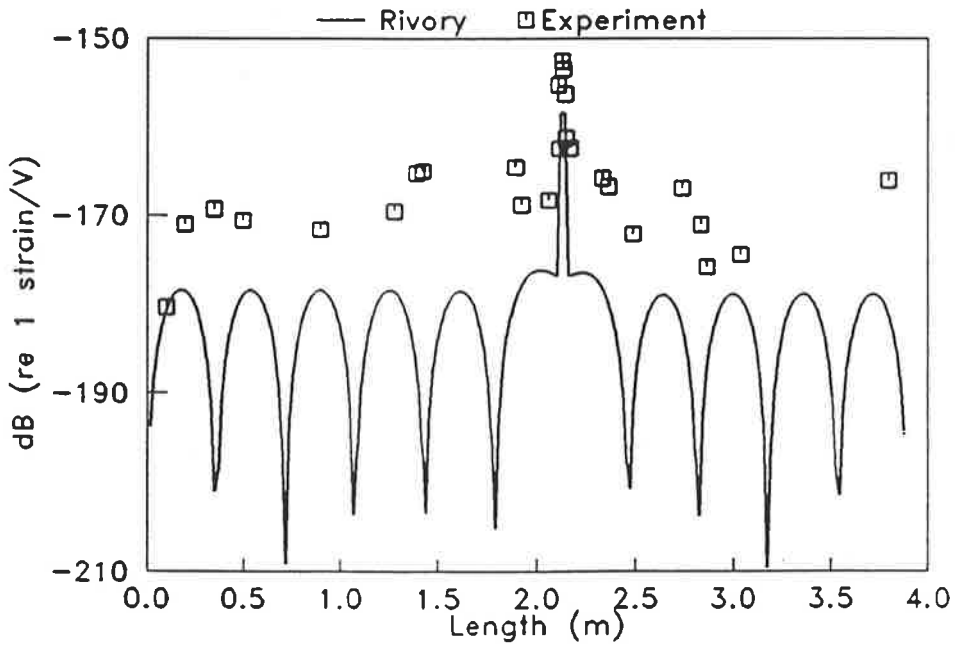

Figure 30. Strain mode shape for f=450 Hz

4.0 POWER FLOW AND COUPLING EFFICIENCY FOR A THIN BEAM

4.1 Theory of power flow measurements in beams

4.1.1 Flexural wave power flow measurements

For one-dimensional flexural wave propagation, the instantaneous power flow, $P_x(x,t)$, in terms of the displacements normal to the beam surface, w, can be described by the following:

$$P_x(x,t) = E_b I_b \left[\left(\frac{\partial^3 w}{\partial x^3} \right) \frac{\partial w}{\partial t} - \left(\frac{\partial^2 w}{\partial x^2} \right) \frac{\partial^2 w}{\partial t \partial x} \right] \tag{56}$$

where:

$$\left(\frac{\partial^3 w}{\partial x^3} \right) \frac{\partial w}{\partial t}$$

represents the force component of the intensity and

$$\left(\frac{\partial^2 w}{\partial x^2} \right) \frac{\partial^2 w}{\partial t \partial x}$$

represents the moment component.

Equation (56) can be further reduced into measurable quantities using finite difference approximations and averaged over time, and thus becomes:

$$<P_x>_t \approx \frac{E_b I_b}{\Delta^3}\left[\left\langle \dot{w}_2(4w_3 - w_4)\right\rangle_t - \left\langle \dot{w}_1 w_3\right\rangle_t\right] \qquad \textbf{(57)}$$

Where $<A>_t$ is the time average value of A, $\dot{G}$ is the first derivative of G with respect to time, and Δ is the spacing between the accelerometers.

Thus the time averaged one dimensional power flow can be measured at one point using a linear array of four accelerometers and suitable analog components, such as summators and integrators. Equation (57) is further reduced in the far-field since, as shown previously, the force or moment components of intensity are each equal to half of the total intensity (Noiseux, 1970). Thus, the total intensity can be found using finite difference approximations to calculate the moment component of intensity, and doubling the result. Hence equation (57) becomes:

$$<P_x>_t = \frac{2\sqrt{(E_b I_b m_b{}')}}{\Delta\ \omega}<\ddot{w}_1\dot{w}_2>_t \qquad \textbf{(58)}$$

Since:

$$\frac{\partial^2 w}{\partial x^2} = -k^2 w \qquad \textbf{(59)}$$

where the wave number, k is:

$$k = \omega\left(\frac{m_b'}{E_b I_b}\right)^{\frac{1}{2}} \tag{60}$$

Hence the time average one dimensional far-field power flow can be measured at one point using a linear array of two accelerometers and suitable analog components (Pavic, 1976).

Cross spectral density measurements enable the evaluations of the time average products contained in equations (57) and (58) (Verheij, 1980). Further advantages of spectral based analysis is that time averaged time derivatives and integrals become either the real or the imaginary part of the cross spectrum multiplied by a constant. Thus, for broadband signals, equations (2) and (3) become respectively:

$$\langle P_x \rangle_t = \frac{E_b I_b}{\Delta^3}\left[4\int_0^\infty \frac{\mathrm{Im}\{G(a_2,a_3,f)\}}{\omega^3}\,df - \int_0^\infty \frac{\mathrm{Im}\{G(a_2,a_4,f)\}}{\omega^3}\,df - \int_0^\infty \frac{\mathrm{Im}\{G(a_1,a_3,f)\}}{\omega^3}\,df\right] \tag{61}$$

$$\langle P_x \rangle_t = 2\frac{\sqrt{(E_b I_b m_b')}}{\Delta}\left[\int_0^\infty \frac{\mathrm{Im}\{G(a_2,a_1,f)\}}{\omega^2}\,df\right] \tag{62}$$

Where $G(a_2,a_3,f)$ is the cross spectral density of the product $a_3\ a_2^*$ where * defines the complex conjugate, and $Re\{G(..)\}$ and $Im\{G(..)\}$ are respectively the real and imaginary parts of the cross spectral density.

And for sinusoidal signals:

$$\langle P_x \rangle_t \approx \frac{E_b I_b}{\Delta^3}\left[\frac{4\mathrm{Im}\{G(a_2,a_3,f)\}}{\omega^3} - \frac{\mathrm{Im}\{G(a_2,a_4,f)\}}{\omega^3} - \frac{\mathrm{Im}\{G(a_1,a_3,f)\}}{\omega^3}\right] \quad \textbf{(63)}$$

$$\langle P_x \rangle_t = \frac{\sqrt{(E_b I_b m_b')}}{\Delta\omega^2}\mathrm{Im}\{G(a_2,a_1,f)\} \quad \textbf{(64)}$$

The quantities in equation (56) can also be estimated by using two strain gauges and two accelerometers, (Carles *et al.*, 1983). This approach is possible since strain is already the second spatial derivative of displacement, as shown in equation (26). Hence for sinusoidal signals:

$$\langle P_x \rangle_t = \frac{2E_b I_b}{t_b \Delta}\left[\frac{\mathrm{Im}\{G(\varepsilon_1,a_2,f)\}}{\omega} - \frac{\mathrm{Im}\{G(\varepsilon_2,a_1,f)\}}{\omega}\right] \quad \textbf{(65)}$$

4.1.2 Power flow in electrical devices

The instantaneous electrical power flow into the piezoelectric actuator can be evaluated by using the measured values of voltage and current, according to the following:

$$P_e = V\, I\, \cos\phi \quad \textbf{(66)}$$

where ϕ is the phase angle between the voltage, V, and the current, I.

The value of time averaged or active power, using cross spectrum analysis can be determined using:

$$\langle P_e \rangle_t = \text{Re } G(V,I,f) \tag{67}$$

4.1.3 Mechanical power flow using a force transducer and an accelerometer

The instantaneous mechanical power flow can also be measured by using force and velocity measurements, and by definition is:

$$P_m = F\ v\ \cos\phi \tag{68}$$

where ϕ is the phase angle between the force, F, and the velocity, v.

The value of time averaged or active power, using cross spectrum analysis can be evaluated by:

$$\langle P_m \rangle_t = \text{Re } G(F,v,f) \tag{69}$$

4.1.4 Coupling efficiency

The coupling efficiency for an actuator can be defined as the ratio of output to input power. Thus, coupling efficiency, ς_c, is:

$$\zeta_c = \frac{\langle P_m \rangle_t}{\langle P_e \rangle_t} \text{ or } \frac{\langle P_x \rangle_t}{\langle P_e \rangle_t} \tag{70}$$

4.2 Power flow measurements in a thin beam excited by piezoelectric actuators

4.2.1 Experimental set-up

For a beam such as the one shown in Figure 7, the power flow field is very reactive and the whole beam can be shown to be significantly affected by near-field effects, since the length of the beam is comparable to the wavelength of the vibration of interest. For this beam the flexural wave-speed at 600 Hz is approximately 100 m/sec and the wavelength is approximately 180 mm. Thus the beam was instrumented with two four accelerometer spatial arrays as shown in Figure 31. It has been shown by Hayek *et al.* that the magnitude error in a power measure is minimised when accelerometer spacings are equal to a twentieth of a wavelength. Thus, an accelerometer spacing of 9 mm was chosen for the measurement array, as at this value represents a twentieth of the wavelength.

Although the measurement array will have it least magnitude error around 600 Hz, frequency sweeping was again used to obtain some idea of power flow in a broad range of frequencies. The ability of the analyser to control the input actuator voltage from the resulting output strain values, enabled the extension of the experimental dynamic range to beyond 80 dB, while maintaining adequate signal to noise ratio. To measure the power flow through the beam a total of six cross spectra need to be measured. Initial experiments showed the results to be stable and repeatable. Thus the following methodology was used. At any one time an accelerometer pair were selected, and the cross spectrum measured. This data was stored in the personal computer, and another accelerometer pair was chosen. The process was repeated until all the required data had been obtained. Power flow at any

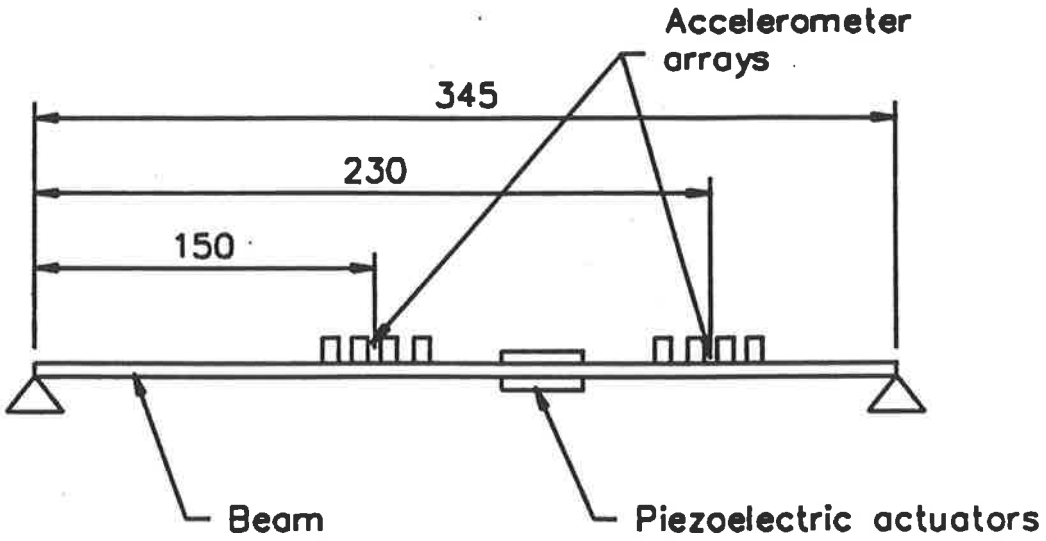

Figure 31. Experimental set-up

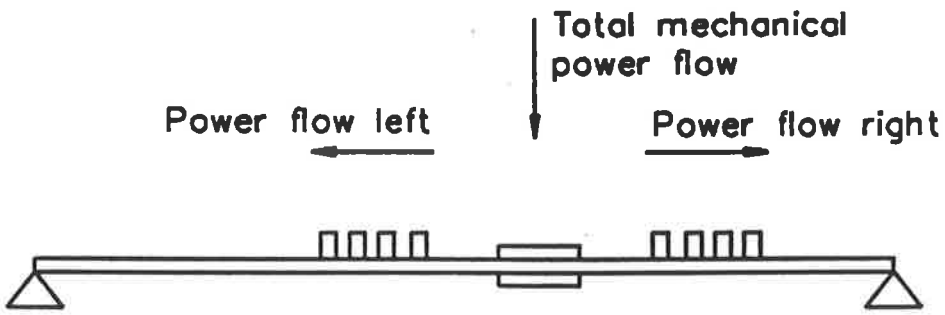

Figure 32. Total mechanical power flow as a sum of the left and right components

frequency could be calculated by manipulating the data stored within the personal computer.

Total mechanical power flow can be defined as the power measured leaving the actuator from its left side plus the power measured leaving the actuator from its right side (see Figure 32). The power provided to the actuator has to be measured before the amplification stage through the step-up transformer, because after the voltage step-up transformer (ratio 38.1:1) the current levels are much too low for accurate measurements.

A 0.1 Ohm precision resistor was placed in series with the power circuit, and current measurements were obtained by measuring the voltage drop across the resistor (see Figure 33).

4.2.2 Results and discussion

Figure 34 shows the results of power measurements obtained during a number frequency sweeps, each lasting approximately 5 minutes, from 300 to 800 Hz. Power flow is greatest at resonances, and much less at frequencies away from resonances. This is to be expected, as real or active power implies that a nett power flow must exist, and in such a reactive system, the only significant energy dissipation will occur at frequencies with large displacements, hence at resonant frequencies.

Coupling efficiency, shown in Figure 35, is defined as the ratio of output mechanical power flow divided by input electrical power. Results of this calculation shows maximum coupling efficiency levels for the third and fourth vibration modes of 48% and 13% respectively. Elsewhere the coupling efficiency is low (from 0.0004% to 0.5%).

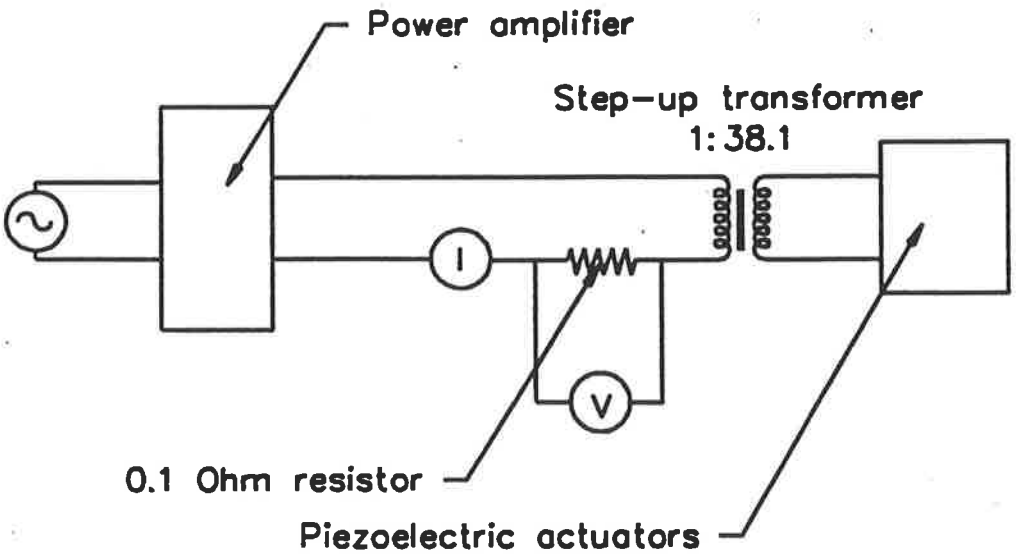

Figure 33. Electrical power measurement set-up

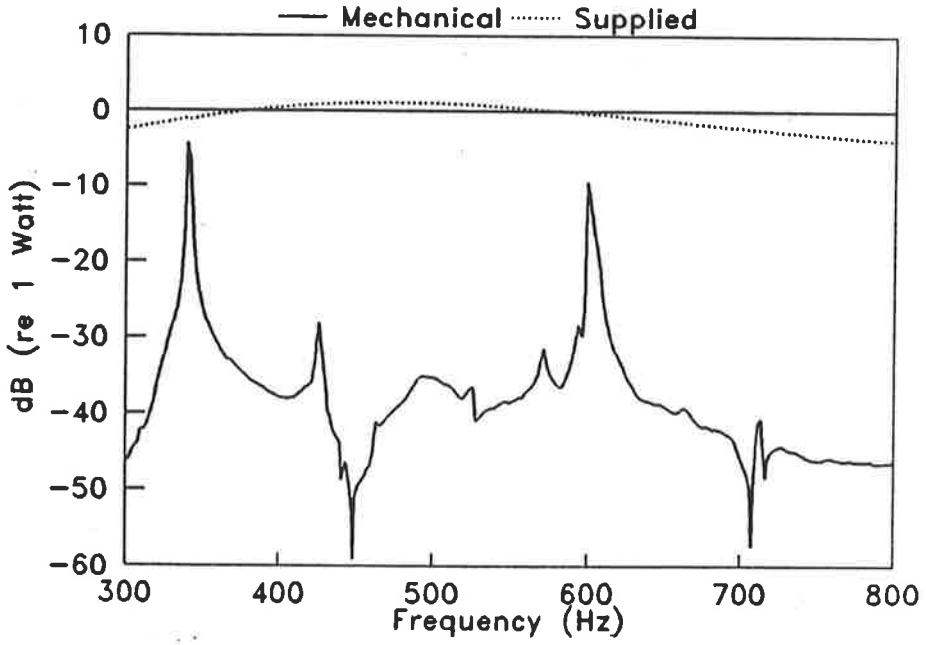

Figure 34. Power flow measurement results

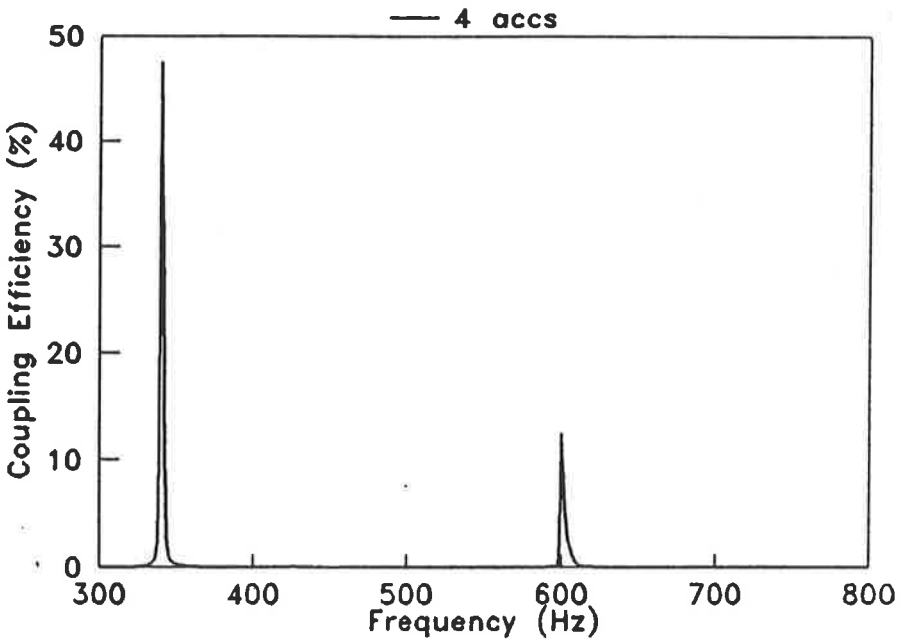

Figure 35. Coupling efficiency

4.3 Power flow measurements in a thin beam excited by an electromagnetic shaker

4.3.1 Experimental set-up

To compare the performance of piezoelectric actuators with that of electromagnetic shaker, the piezoelectric actuators of the beam shown in Figure 31 were replaced by an electromagnetic shaker, as shown in Figure 36. In addition, a force transducer and accelerometer arrangement was located directly behind the shaker/beam attachment point. This enabled the measurement of mechanical power flow into the beam using a well proven, well understood measurement system. The accelerometer spatial arrays were the same as those used in power flow measurements with the piezoelectric actuators.

4.3.2 Results and discussion

Unlike the piezoelectric actuators, the attachment of the shaker to the beam has major effects on the dynamic response of the beam. The mass loading effects result in the shifting of some of the natural frequencies, while the added armature damping results in larger modal damping. These effects can be seen in the strain results measured at x=150mm shown in Figure 37.

Figure 38 shows the power flow from 200 to 800 Hz. Again active power flows are larger at resonances than at other frequencies. There is good agreement between total mechanical power flow measured using the two four accelerometer arrays and the beam input power measured using the force transducer and accelerometer. There is however more spurious

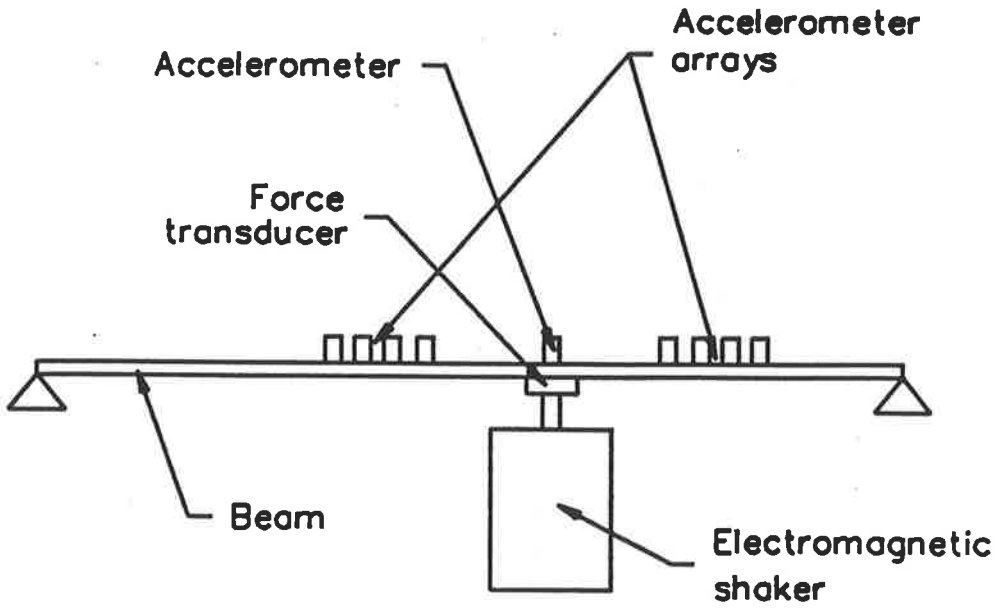

Figure 36. Experimental set-up

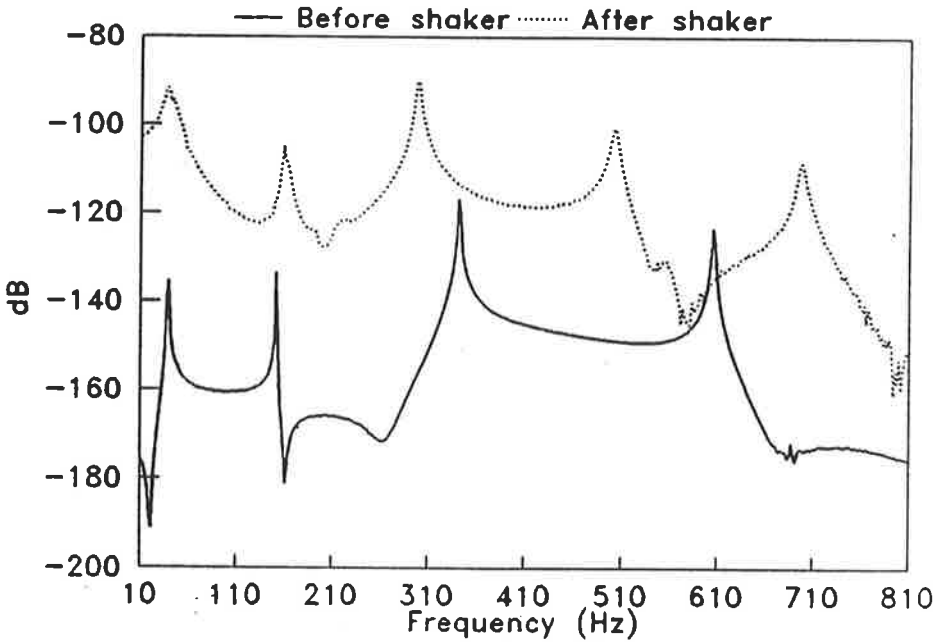

Figure 37. Effects of electrodynamic shaker on the beam response

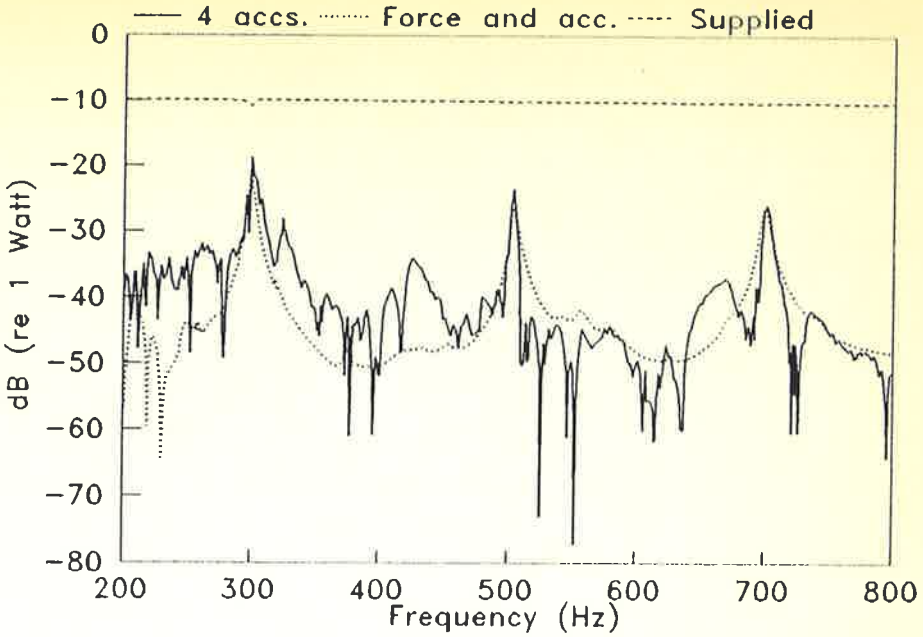

Figure 38. Results from power flow measurements

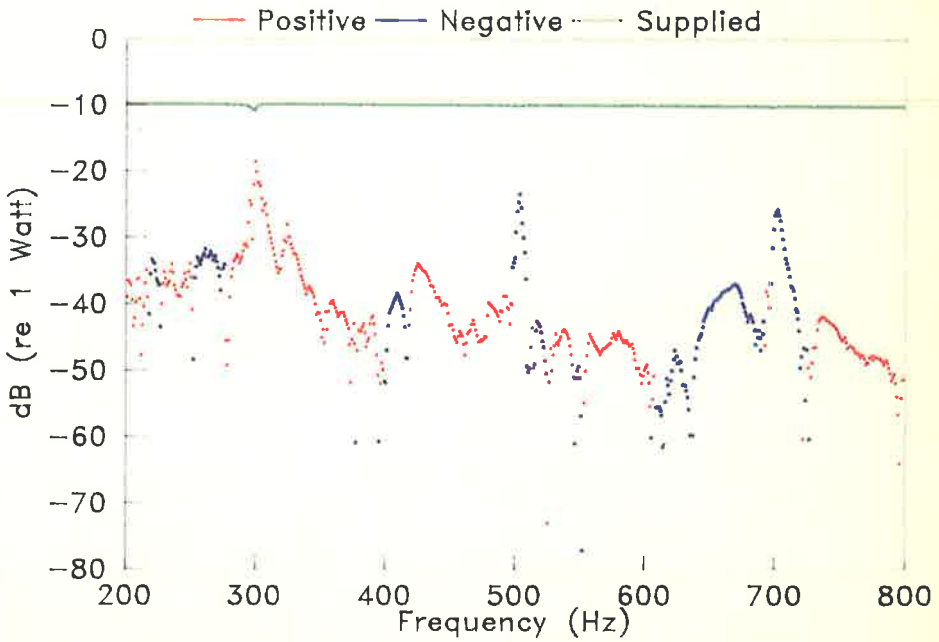

Figure 39. Results from power flow measurements, with positive and negative power flows

data in the results obtained using the four accelerometer arrays. Indeed, if the direction of the power flow is taken into account there are regions where the real power flow, although of a level comparable with the results from the force transducer and accelerometer, is flowing out of the beam rather than into the beam (Figure 39). This of course has no real physical meaning, but indicates errors of the sort mentioned by Taylor, 1990.

The results shown have been repeated a number of times and the following observations can be made:

- Although the measurements were not conducted instantaneously the measured phase between accelerometers was stable and repeatable.

- Coherence in all measurements was good and greater than 0.9.

- There are no doubts that phase errors are a big source of overall errors (Taylor, 1990). The best phase error measured between accelerometers and charge amplifiers in this experiment was 0.2 degrees at 150 Hz.

- The second significant source of errors comes from the fact that at various frequencies, modal nodes or antinodes will be located somewhere within the measurement array. This leads to a large approximation error in the slope estimations required for power flow measurements. These errors again have been shown by Taylor, 1990, not to be negligible.

- Lastly, since the reflection coefficient (defined as the ratio of the travelling wave amplitude to the reflected wave amplitude) for this beam is close to one, or since the reverberation time is long, the presence of standing waves (large reactive power flow) will tend to obscure the lower active power flow (Taylor, 1990).

- Despite these errors, it can be seen from Figures 38 and 39 that, broadly speaking, the power measurements obtained by the two different methods are in agreement. Some frequency smoothing could perhaps improve the results.

The coupling efficiency, for this experiment (Figure 40), has efficiencies reaching 10-15% at resonance and 0.01% to 1% off resonance. Thus coupling at resonance is highest for the piezoelectric actuators, with efficiencies reaching 48% compared to 15% maximum reached by the shaker. Off-resonance, the shaker efficiencies although small (from 0.01% to 1%), are larger than those achieved by the piezoelectric actuators (from 0.0004% to 0.5%).

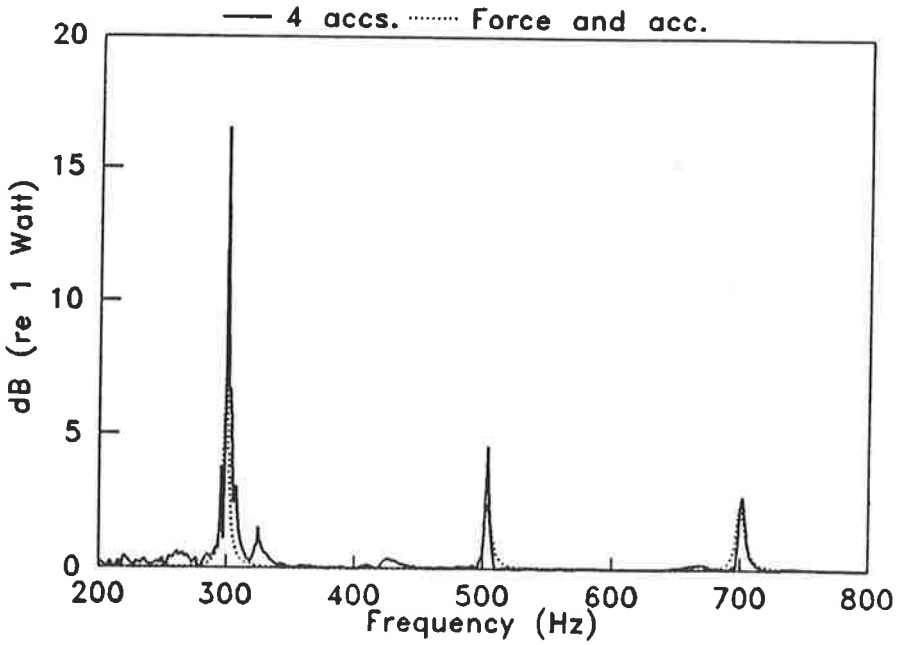

Figure 40. Coupling efficiency

5.0 OTHER CONSIDERATIONS

5.1 Piezoelectric actuator failures

Throughout the experimental program continual failure of the piezoelectric actuators caused considerable difficulty, and the following anecdotal notes are intended for future users.

A total of eleven (11) actuators were used throughout the experiments of this study. Out of those eleven (11), seven (7) failed: two (2) deliberately, three (3) on installation, and two (2) during what should be classified as normal usage. Generally, the voltage provided to the actuators was kept well below the upper limit ranges of the coercive voltage (the voltage at which the poling or depoling occurs and for PZT G-1195 approximately equals 240 Volts rms at 60 Hz), in the range of 30 to 120 Volts rms within the frequency range 10 to 1000 Hz. Furthermore, the feedback control capability of the HP3562A analyser allowed the output strain levels on the beams to be kept to within safe bounds. Hence, the actuators where not subjected to any worse conditions that they would be subjected to in the field.

The two (2) deliberately failed actuators were subjected to a level exceeding 400 Volts rms at 550 Hz (see Figures 41 and 42). This frequency was chosen as it did not coincide with a resonant mode, hence lower strain levels would be reached for a given voltage input. The main failure mechanism for these actuators were surface cracks, which then lead to electrical break-down. During the electrical break-down, a miniature lightning

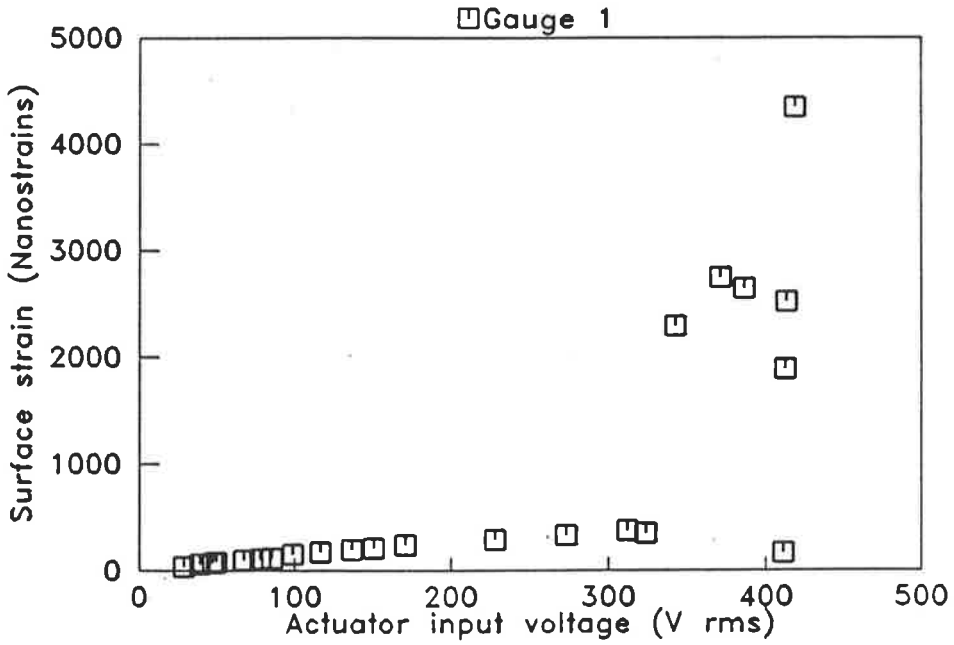

Figure 41. Surface strain versus input actuator voltage up to destruction (f=550 Hz)

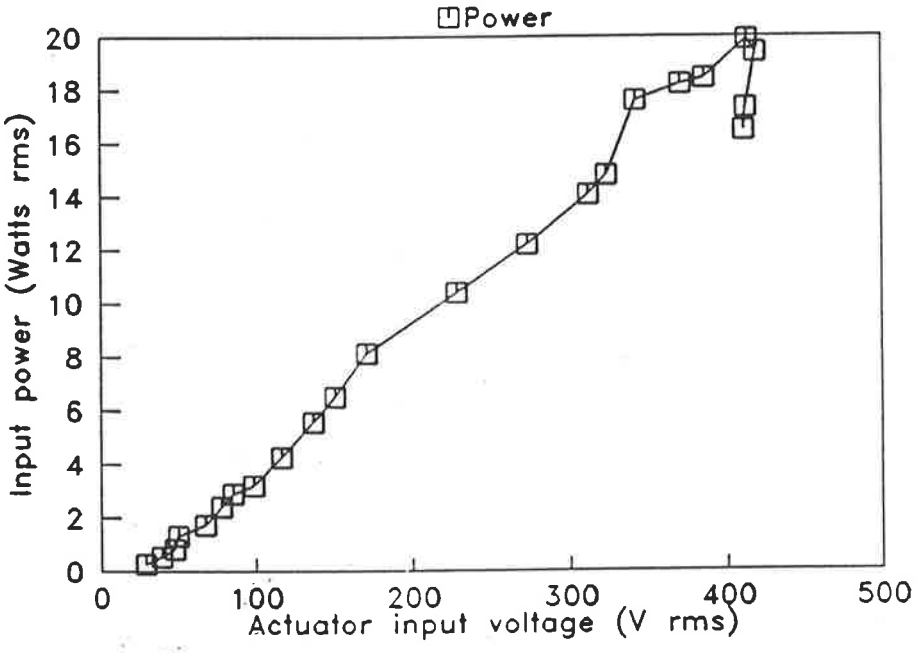

Figure 42. Input power versus input actuator voltage up to destruction (f=550 Hz)

storm could be observed over the surface of the failed actuators.

Three (3) actuators failed on installation. They all had some response at low voltage inputs but then tended to behave erratically at the required higher input voltage levels. Their behaviour was reminiscent of the high voltage break-down effect, and it was felt (but not proven) that the break-down was either somewhere around the perimeter of the piezoelectric actuator or between the base layer of the actuator and the beam.

Two actuators failed during what can only be classified as normal usage. The first failure occurred after about six months of intermittent but regular use. A lateral crack appeared on the actuator and its performance was badly affected. It was felt (not proven) that the failure represented a mechanical failure of the actuator, somewhat like the actuator had been bent too far. The progress of the second failure, by luck, was observed quite closely. A small longitudinal crack appeared on one edge of the crystal. This crack could be seen quite easily due to the electrical sparks spanning that crack. Slowly at first and then quite rapidly the longitudinal crack grew the full length of the crystal. The team at the University of Adelaide had been trying different "on-the-run" methods of repair. A promising method was to coat the cracks with a high conductive paint, Electrodag-915. This appeared to allow the electrical connection between the piezoelectric segments on either side of the cracks, without shorting the connection between the layers. This crystal was successfully repaired and worked at pre-cracking performance levels. That is until quite abruptly, something exploded with a flash and a bang. This was most perturbing, particularly as the actuator at the time was not actually being used, although connected to the power source. Closer inspection of the actuator surface revealed that the silver patch

had scorched in a localised region on top of the existing crack. The conclusion reached was that some continuous charging (but no discharging) of some localised part of the crystal had been taken place over a period of time, until some sort of saturation was reached and exceeded. The actuator was cleaned, repaired and observed to work. However, closer measurements showed that its performance had deteriorated, for its phase response had shifted by some 20°. The actuator had been instantly depoled and repoled to some odd poling direction. This actuator was hence replaced.

The above testimonies are not meant to be taken as an in-depth performance survey of piezoelectric devices and materials, but remain purely the observations of what actually took place during the various experiments undertaken. Only one batch of PZT G-1195 material was used though the experiments. Although other experimental rigs have suffered similar fates.

5.2 Actuator voltage linearity

Tests have shown that over a range the piezoelectric actuator force output is linear with the input voltage. Both input power (Figure 42) and output strain levels (Figure 43) are essentially linear with the input voltage within the range 0 to 200 V rms, but become increasingly non-linear above this voltage, as is expected since this value approaches the coercive field.

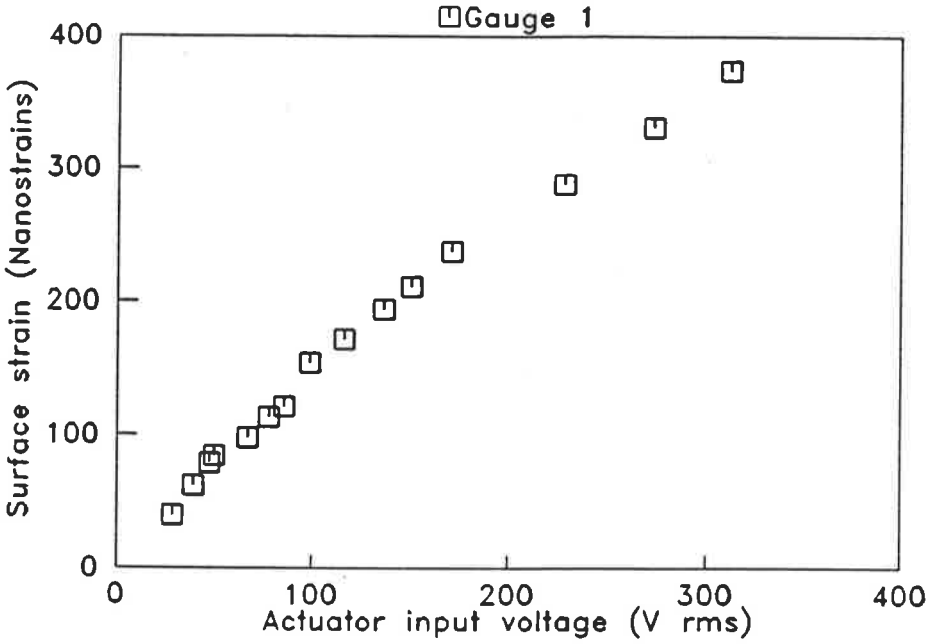

Figure 43. Linearity of surface strain versus input actuator voltage (f=550 Hz)

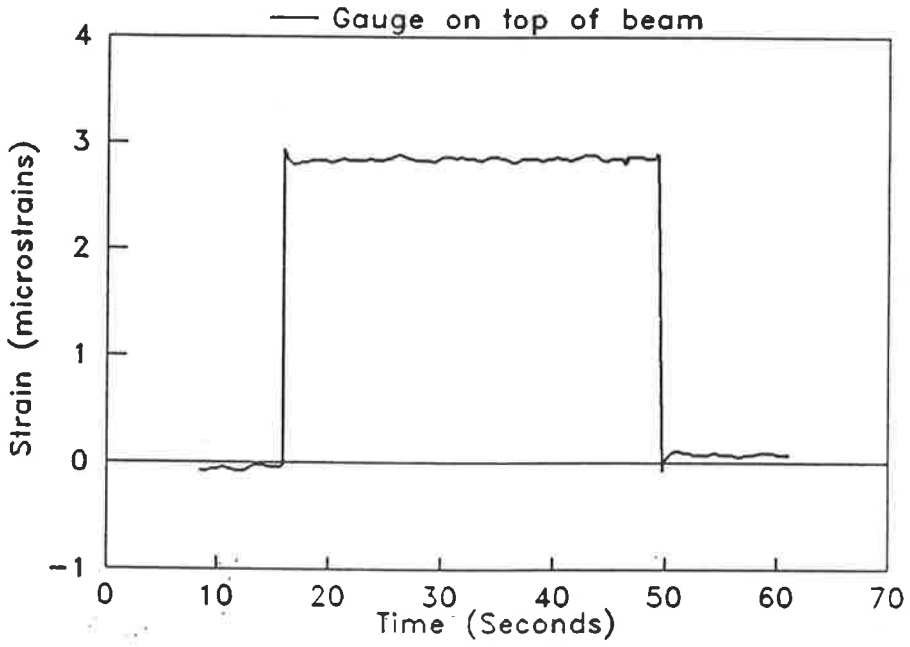

Figure 44. DC response of strain gauge on beam

5.3 Actuator leakage

During some of the calibration measurements, an interesting phenomenon was noted. The calibration measurements involved using some calibrated weights to deflect an instrumented thin beam. The strain values registered by the strain gauges on the top surface of the beam were compared to values obtained by classical Bernoulli-Euler beam theory. For gauges on the beam surface, the application of the weights was registered as a DC shift on the chart recorder (see Figure 44). Figure 45 shows that for gauges on top of the piezoelectric actuator, the initial peak strain value which was reached decayed exponentially over time, the reverse effect was observed with the load removed. This was despite the piezoelectric actuator being open circuit, thus leading to the conclusion that some of the charge developed must leak away. This does not pose a threat to any high frequency operation of piezoelectric actuators, but for any operation below 5 Hz it may have serious consequences, such as large time lags between the applied voltage and the force response.

5.4 Actuator non-linearities

Despite the linear behaviour exhibited by the piezoelectric actuator over the voltage input range shown in Section 5.2, piezoelectric actuators do exhibit non-linear characteristics in the frequency spectrum of their output for any given input. Generally, the frequency content of the input and the output was the same. On occasions, however, the frequency content of the output included high level harmonics of the fundamental, which became more noticeable as the piezoelectric actuator was driven at higher levels.

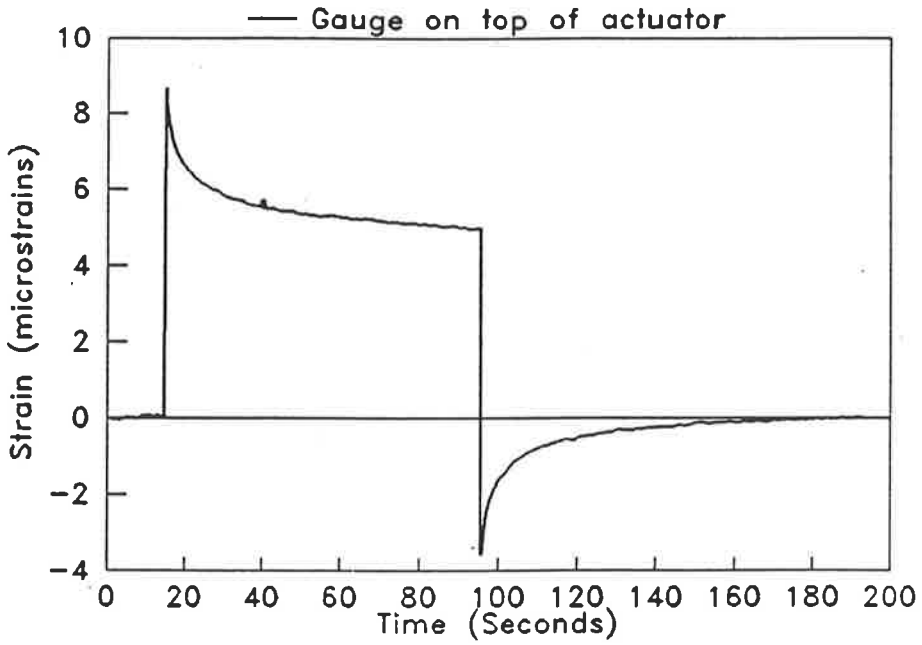

Figure 45. DC response of strain gauge on piezoelectric actuator

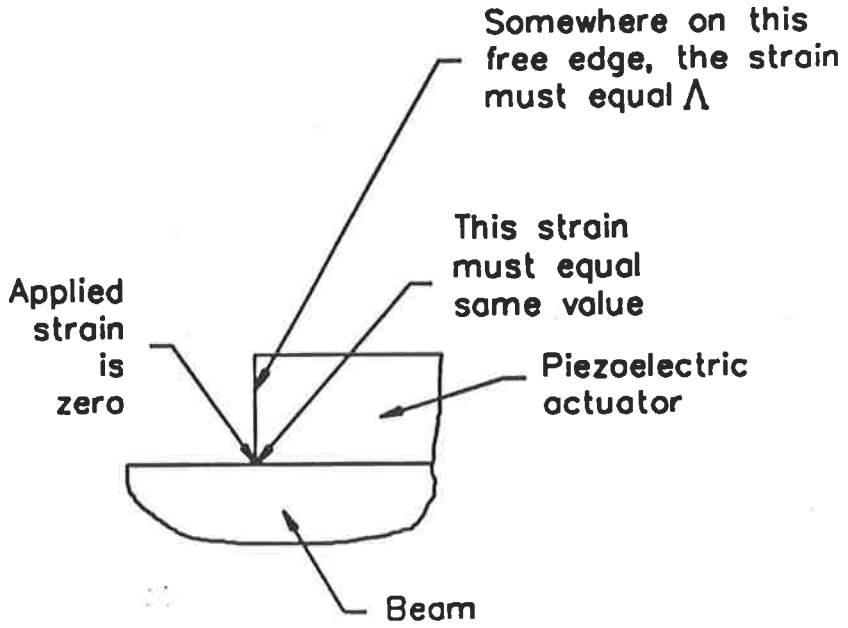

Figure 46. Strain singularity

5.5 Shear lag - strain singularity

Figure 46 duplicates a previous figure showing the point where the strain singularity occurs. As mentioned in Section 3.3, this singularity is responsible for the increase actuator strain near to the end of the actuator. The shear lag mechanism is sometimes described in advanced mechanics texts (Peery, 1950) and has been alluded to by Crawley and de Luis, 1987.

The free edge condition of the piezoelectric actuator necessitates the stress free boundary condition. Then by equation (5), the applied strain at the free edge must equal Λ. However as mentioned previously the applied strain, just on the beam side of the actuator, is zero, hence the strain singularity. Thus there must be relative displacement, and hence shearing strain, between the beam and the actuator at the interface. At distances further and further removed from the free edge, the shear strain reduces more and more, until there will not be any shear strain between the piezoelectric actuator and the beam. This is the only manner by which the strain singularity can be explained. Timoshenko and Goodier, 1951, tried to solve what is a similar problem, albeit a static analogy: a three (3) dimensional bar hanging loaded by its own weight. At the boundary, with no displacements allowed, there exists a strain singularity between the bar and its support. Timoshenko's solution to this problem, although correct at some distance away from the strain singularity, is not correct at the boundary, for the solution allows displacements to occur at the boundary.

With this particular problem in mind, a solution for a two (2) dimensional bar hanging under static self weight was sought after. It was felt that such a solution would go a long

way towards explaining the strain singularity - shear lag mechanism. Although finding an exact solution to the two dimensional differential equations describing the stress field throughout the bar was unlikely, it was felt that a polynomial approximation might be found to satisfy the differential equations of equilibrium, together with the compatibility equation and the boundary conditions. This proved difficult as with all the boundary conditions equal to zero, all the polynomial coefficients soon trivialised to zero. Lastly, it was thought that some of the boundary conditions should be changed to a minimum rather an absolute zero, to try and stop the trivialisation of the answer. Thus, the strain energy on the surface away from the surface of interest was minimised. Initial results from this solution method were discouraging, and with time running short the solution to this problem was regrettably abandoned. It is believed that a similar approach or perhaps one based on the calculus of variation may be able to solve this interesting problem.

6.0 CONCLUSIONS AND RECOMMENDATIONS

A new model, based upon work reported by Pan *et al.* (1992), which calculates the response of a simply supported beam excited by a pair of piezoelectric actuators bonded to opposite sides has been presented in Section 3.2, and theoretical predictions have been verified experimentally. It has been shown that the results of this model (which divides the beam into three separate segments) are equivalent to those obtained using the model of Clark *et al.* (1991). It was also found that the stiffness and inertia added to the beam by the actuators had a negligible effect on the results.

Two different mechanisms for transferring the force from the actuator to the beam were shown to exist. The first mechanism involves force transfer by way of either equivalent line moments or a uniform strain distribution over the actuator/beam interface. Results obtained with a theoretical model using this mechanism as a basis agree well with experiment at beam resonance frequencies, but not at frequencies between resonances. This lack of agreement at non resonance frequencies is due to the domination of the force transfer by a second mechanism in which the strain field at the free edge of the actuator/beam system affects the dynamic behaviour of both systems. In this mode, the actuator strain field is markedly different to that of the beam and is clearly dependent on the impedance of the sub-system on which it is acting. The actuator strain field in this mode is reminiscent of the shear lag mechanism identified by Crawley and de Luis (1987), where the rapid change in strain near the free edge of the actuator results in a large increase of shear strain. This force transfer mechanism is obviously less efficient than the first. Therefore, the free edge condition of the piezoelectric actuator does not affect the

beam's dynamic response at resonance, but the free edge condition does affect its dynamic response at other frequencies. Thus the free edge condition of the piezoelectric actuator does affect the dynamic response of the actuator and the beam, and this effect must be taken into account.

The existing one dimensional model of the beam section containing the actuator is clearly inadequate to describe the near-field actuator/beam response and the beam response at non-resonance frequencies. A better model could use a similar approach as used in this paper (dividing the beam into three sub-systems) but a two or three dimensional model of the actuator/beam sub-system will be required.

The strain values under the actuators are shown to exceed values elsewhere in the structure, but that strain value will never exceed the value of the calculated applied strain assumed pure bending for that is the more efficient transfer mechanism. Yet, the value of strain reached on the surface of the actuator has been shown to vary considerably depending upon the force transfer mechanism, and this must be taken into account when designing active control systems.

The power flow experiments (Section 4.0) clearly show that the piezoelectric actuator is by far more efficient (approximately 48%) in converting electrical energy into mechanical energy (definition for coupling efficiency) than the electromagnetic shaker (approximately 15%) at beam resonances. In this case, the force transfer mechanism from the piezoelectric actuators, is efficient. Away from resonances, the coupling efficiency of both methods drops rapidly to small values with the electrodynamic shaker (from 0.01% to 1%) yet far

more efficient than the piezoelectric actuator (from 0.0004% to 0.5%). The force transfer mechanism for the piezoelectric actuators is thus far less efficient away from resonance.

It was found difficult to obtain accurate power flow measurements. There are a number of factors (the accelerometer spacing itself, accelerometer spacing tolerance, phase matching between accelerometers and indeed between measurement channels, and reverberation time of the structure being measured) which act together to compound the error, and furthermore as the error resulting from one factor is minimised, the error component for another factor increases. Further, the finite difference arrays utilised are designed to operate accurately only over a limited specific frequency range, and the mass loading of the accelerometers is not negligible for light structures.

REFERENCES

Bailey, T., and Hubbard, Jr., J. E. 1985. "Distributed piezoelectric-polymer active vibration control of a cantilever beam", Journal of Guidance, Vol. 8, No.5.

Baz, A., and Poh, S. 1988. "Performance of an active control system with piezoelectric actuators", Journal of Sound and Vibration, 126, pp 327-343.

Burke, S. E. , and Hubbard, Jr., J. E. 1987. "Active vibration control of a simply supported beam using a spatially distributed actuator", IEEE Control Systems Magazine, pp 25-30.

Burke, S. E., and Hubbard, Jr., J. E. 1988. "Distributed actuator control design for flexible beams", Automatica, Vol. 24, No. 5, pp 619-627.

Carles C., Villenave, M., Alaphillippe, M., and Pascal J. C. 1983. "Mesure de l'intensité vibratoire et du coefficient de transmission dans les barres", 11^{e} ICA, Paris.

Clark, R. L., Fuller, C. R., and Wicks, A. 1991. "Characterisation of multiple piezoelectric actuators for structural excitation", Journal of the Acoustical Society of America, 90(1), pp 346-357.

Craig Jr., R. R. 1981. "Structural dynamics: an introduction to computer methods", John Wiley & Sons, USA.

Crawley, E. F., and de Luis, J. 1987. "Use of piezoelectric actuators as elements of intelligent structures", AIAA Journal, Vol. 25, No. 10, pp 1373-1385.

Crawley, E. F., and Anderson, E. H. 1990. "Detailed models of piezoceramic actuation of beams", Journal of Intelligent Material Systems and Structures, Vol. 1, pp 4-25.

Dimitriadis, E. K., Fuller, C. R., and Rogers, C. A. 1991. "Piezoelectric actuators for distributed vibration excitation of thin plates", Transactions of the ASME, Journal of Vibration and Acoustics, Vol. 113, pp 100-107.

Fuller, C. R., Rogers, C. A., and Robertshaw, H. H. 1989. "Active structural control with smart structures", Paper presented at SPIE Conference 1170 on Fiber Optic Smart Structures and Skins II, Boston, MA.

Hansen, C. H., and Pan., J. 1990. "Active control of vibration in a beam", Proceedings of The Institution of Engineers Australia Vibration and Noise Conference, Melbourne, pp 334-338.

Hayek, S. I., Pechersky M. J., and Suen B. C. 1990. "Measurement and analysis of near and far field structural intensity by scanning laser vibrometery", CETIM International Congress on Intensity Techniques, August 1990, pp 281-288.

Kim, S. J., and Jones, J. D. 1991. "Optimal design of piezoactuators for active noise and vibration control", AIAA Journal, Vol. 29, No. 12, pp 2047-2053.

Kino, G. S. 1987."Acoustic waves: Devices, imaging, and analog signal processing", Prentice-Hall inc., USA.

Liang, C., and Rogers, C. A. 1989. "Behaviour of shape memory alloy actuators embedded in composites", Proceedings of the 1989 Composites Conference, Beijing, China.

Liao, C. Y., and Sung, C. K. 1991. "Vibration suppression of flexible mechanisms using piezoelectric sensors and actuators", Journal of Intelligent Material Systems and Structures, Vol. 2, pp 177-197.

Noiseux, D. U. 1970. "Measurement of power flow in uniform beams and plates", Journal of the Acoustical Society of America, 47, pp 238-247.

Pan, J., and Hansen, C. H. 1989. "Active control of total vibratory power flow in a beam: I. Physical system analysis", Journal of the Acoustical Society of America, pp 200-209.

Pan, J., and Hansen, C. H. 1990. "Active control of total power flow along a beam", Proceedings of the International Congress on Recent Developments in Air- and Structure-borne Sound and Vibration, Auburn University, USA, pp 229-236.

Pan, J., Hansen, C. H., and Snyder S. D. 1992. "A study of the response of a simply supported beam to excitation by a piezoelectric actuator", Journal of Intelligent Material Systems and structures, Vol. 3, pp 3-16.

Pavic, G. 1976. "Measurement of structure borne wave intensity, Part I: Formulation of the methods", Journal of Sound and Vibration, 49, pp 221-230.

Peery, D. J. 1950. "Aircraft structures", McGraw-Hill Book Co., Inc., USA.

Rogers, C. A., Liang, C., and Jia, J. 1991. "Structural modification of simply-supported laminated plates using embedded shape memory alloy fibers", Computers and Structures, Vol. 38, No. 5/6, pp 569-580.

Taylor, P. D. 1990. "Nearfield structureborne power flow measurements", International Congress on Recent Developments in Air- and Structure-Borne Sound and Vibration, Auburn University, USA, pp 339-345.

Thompson W. T., 1981. "Theory of vibration with applications", George Allen and Unwin, Great Britain.

Timoshenko S. and Goodier J. N., 1951. "Theory of elasticity", Mc Graw-Hill Book Co., USA.

Verheij, J. W. 1980. "Letters to the editor: Cross spectral density methods for measuring structure borne power flow on beams and pipes", Journal of Sound and Vibration, 70, pp 133-139.

Wang, B., Dimitriadis, E. K., and Fuller, C. R. 1990. "Active control of structurally radiated noise using multiple piezoelectric actuators", AIAA Paper 90-1172.

LIST OF SYMBOLS

b_b	beam width
Δb_c	change in actuator width
b_c	actuator width
D	electric displacement
d	piezoelectric stress constant
d_{31}	piezoelectric stress constant - transverse charge coefficient
d_{33}	piezoelectric stress constant - axial charge coefficient
E_b	Young's modulus of beam
E_c	Young's modulus of piezoelectric crystal
I_b	beam second moment of area
k	bending wave number in beam
K	coefficient defined by equations (14), (17) or (21)
ΔL_c	change in actuator length
L_c	actuator length
L_x	beam length
m'_b	mass per unit length of beam

M_x	internal beam moment
M_z	applied external line moment
P	coefficient defined by equations (13), (16) or (20)
P_e	electrical power flow as measured using current and voltage
P_m	mechanical power measured using force and acceleration transducers
P_x	power flow in beam using accelerometers
R	beam curvature
S	beam internal shear force
t	time
t_b	beam thickness
Δt_c	change in actuator thickness
t_c	actuator thickness
$u^s{}_b$	beam surface displacement in x direction
V	Voltage applied to piezoelectric crystal
w	beam vertical displacement
$x\ y\ z$	coordinate system
$x_1\ x_2$	actuator locations

Subscripts

b	beam
b1 b2 b3	sub beams 1 2 3
c	actuator (crystal)

Greek

Δ	accelerometer spacing in finite difference schemes
ε_c	actuator strain at any x
ε^s_b	beam surface strain
ε^s_a	distributed strain applied to the beam surface
ζ_c	coupling efficiency
η_b	beam loss factor
η_c	actuator loss factor
θ	angular rotation of the beam plane perpendicular to the beam axis (x-axis)
Λ	actuator strain due to the electric field only

ν_b	beam Poisson's ratio
ν_c	actuator Poisson's ratio
ϱ_b	beam density
ϱ_c	crystal density
σ_b	beam stress at any point
$\sigma^s{}_b$	beam surface stress
σ_c	actuator stress at any point
σ_x	beam stress in x direction
Ψ_b	Beam to actuator stiffness ratio
ω	angular frequency

Errata - Thesis: Dynamic Response of Simply supported Beams by Piezoelectric Actuators - By: J. Rivory

ERRATA

P. 5	Line 10	"thesis" should replace "paper"
p. 24	Line 4	"ten (10) boundary conditions" should read "twelve (12) boundary conditions"
p. 26	Line 1	"equations (41) to (42)" should read "equations (41) to (52)"
p. 26	Equation (52)	"$\int e$" should be replaced by "$\int \varepsilon$"
p. 36	Line 4	"where" should be replaced by "were"
p. 36	2nd para	"There is also very good agreement between both the Clark *et al.* (1990) model, the model postulated here and the experimental data at all measurement points (see Figures 11, 12, and 13)." should read "There is also very good agreement between both the Clark *et al.* (1990) model, and the model postulated here at all measurement points (see Figures 11, 12, and 13)."
p. 36	2nd para	The following should be read as being inserted between the second and third paragraph.

Furthermore, it can be shown using transformed section theory, that the EI of the beam section is increased by 23% with the addition of the actuator stiffness. But that at the same time, the linear mass of the beam section is increased by 19%. Since the Bernoulli beam equation consists of a stiffness plus a mass term, substitution of stiffness and mass increases into equation (29), gives rise to a negligible mass/stiffness loading of approximately 3% (about 0.3 dB). It should be noted that this is valid for the beam system under study, but that for other beam systems, the mass/stiffness loading may not be negligible.

p. 37	Line 1	"(eg. 420 Hz)" should be amended to read "(eg. 420 Hz in Figures 11, 12, 13, and 17)"
p. 37	Line 7	"18)" should read "17)"
p. 37	Line 12	"log10" should read "$\log_{10}$"

p. 52	2nd Para	"There is good agreement between the model and the experimental results close to the actuator (Figures 3 and 4). At regions far from the actuator, at low frequencies there is good agreement also; however, at higher frequencies, in between the resonance peaks, the agreement is poor (Figures 25 and 26)." has been amended to read "In terms of magnitude, there is a degree of agreement at all frequencies between the model and the experimental results close to the actuator (Figures 23 and 24), but only at low frequencies at regions away from the actuators. In these regions at high frequencies and between the resonance peaks, there is no agreement (Figures 25 and 26)."
p. 52	Line 9	"out phase" should read "out of phase"
p. 57	Lines 3 to 5	Figures 7,8, 9, 10 should read Figures 27,28, 29, 30
p. 57	Line 8	"frequency underestimation" should read "frequency overestimation"
p. 59	Equation (56)	Reference should be made to Pavic (1976) who derives the equation
p. 60	Line 1	"using finite difference approximations" should be amended to "using finite difference approximation such as that used by Pavic (1976)"
p. 60	Line 9	"using finite difference approximations" should be amended to "using the finite difference approximation such as that used by Pavic (1976) and Noiseux (1970)".
p. 61	Equation (60)	"k =" should read "k^2 ="
p. 64	Line 6	"Hayek *et al.*" should read "Hayek *et al.* (1990)"
p. 64	Line 9	"as at this" should read "as this"
p. 64	Line 10	"it" should read "its"
p. 66	Line 11	"number frequencies" should read "number of frequencies"
p. 76	Line 12	"where" should read "were"